European Journal of Medicinal Chemistry 243 (2022) 114746

Contents lists available at ScienceDirect

European Journal of Medicinal Chemistry

journal homepage: www.elsevier.com/locate/ejmech

Research paper

Development of L-Dopa-containing diketopiperazines as blood-brain barrier shuttle

Catia Cornacchia [a], Lisa Marinelli [a], Annalisa Di Rienzo [a], Marilisa Pia Dimmito [a], Federica Serra [a], Giuseppe Di Biase [a], Barbara De Filippis [a], Hasan Turkez [b], Adil Mardinoglu [c,d], Ilaria Bellezza [e], Antonio Di Stefano [a], Ivana Cacciatore [a,*]

[a] Department of Pharmacy, University "G. D'Annunzio", Via dei Vestini 31, 66100, Chieti, Italy
[b] Department of Medical Biology, Faculty of Medicine, Ataturk University, 25240, Erzurum, Turkey
[c] Science for Life Laboratory, KTH, Royal Institute of Technology, 24075, Stockholm, Sweden
[d] Centre for Host Microbiome Interactions, Dental Institute, King's College London, London, SE1 9RT, United Kingdom
[e] Department of Medicine and Surgery, University of Perugia, Polo Unico Sant'Andrea delle Fratte, P.le L. Severi 1, Perugia, 06132, Italy

ARTICLE INFO

Keywords:
Antioxidant
Blood brain shuttle
Brain delivery system
Diketopiperazine
Levodopa
Parkinson's disease

ABSTRACT

In our overall goal to develop anti-Parkinson drugs, we designed novel diketopiperazines (**DKP1-6**) aiming to both reach the blood-brain barrier and counteract the oxidative stress related to Parkinson's Disease (PD).

The anti-Parkinson properties of **DKP 1–6** were evaluated using neurotoxin-treated PC12 cells, as *in vitro* model of PD, while their cytotoxicity and genotoxicity potentials were investigated in newborn rat cerebral cortex (RCC) and primary human whole blood (PHWB) cell cultures. The response against free radicals was evaluated by the total antioxidant capacity (TAC) assay. Comet assay was used to detect DNA damage while the content of 8-hydroxyl-2′-deoxyguanosine (8-OH-dG) was determined as a marker of oxidative DNA damage. PAMPA-BBB and Caco-2 assays were employed to evaluate the capability of **DKP1-6** to cross the membranes. Stability studies were conducted in simulated gastric and intestinal fluids and human plasma.

Results showed that **DKP5-6** attenuate the MPP^+-induced cell death on a nanomolar scale, but a remarkable effect was observed for **DKP6** on Nrf2 activation that leads to the expression of genes involved in oxidative stress response thus increasing glutathione biosynthesis and ROS buffering. **DKP5-6** resulted in no toxicity for RCC neurons and PHWB cells exposed to 10–500 nM concentrations during 24 h as determined by MTT and LDH assays and TAC levels were not altered in both cultured cell types. No significant difference in the induction of DNA damage was observed for **DKP5-6**. Both DKPs resulted stable in simulated gastric fluids ($t_{1/2} > 22h$). In simulated intestinal fluids, **DKP5** underwent immediate hydrolysis while **DKP6** showed a half-life higher than 3 h. In human plasma, **DKP6** resulted quite stable. **DKP6** displayed both high BBB and Caco-2 permeability confirming that the DKP scaffold represents a useful tool to improve the crossing of drugs through the biological membranes.

1. Introduction

Cyclo-dipeptides such as piperazine-2,5-diones, generally reported with the common name of 2,5-diketopiperazines (DKPs), are relatively simple compounds and among the smallest peptidic derivatives found in nature [1]. Marine organisms, yeasts, fungi, and bacteria are a wide source of natural DKPs [2,3]. These simplest natural cyclo-peptides possess remarkable biological activities such as antimicrobial, anti-tumor, antiviral, anti-Alzheimer, and anticancer [4–6].

Compared to linear peptides, cyclic peptides like DKPs have structural features resulting in a better pharmacological profile [7]. The peculiar heterocyclic scaffold of DKPs confers high stability against proteolysis and constitutes a structural requirement for increased cell permeability, higher activity and selectivity, and less cytotoxicity [8]. Moreover, some DKPs can cross the blood-brain barrier via a passive diffusion process as useful new therapeutic agents for brain diseases [9].

The DKP skeleton, consisting of a substituted or not six-membered ring, is attractive for drug design due to its simplicity, conformational

* Corresponding author. Department of Pharmacy, University "G.d'Annunzio" di Chieti-Pescara, via dei Vestini 31, 66100, Chieti Scalo, CH, Italy.
E-mail address: ivana.cacciatore@unich.it (I. Cacciatore).

https://doi.org/10.1016/j.ejmech.2022.114746
Received 7 July 2022; Received in revised form 24 August 2022; Accepted 3 September 2022
Available online 8 September 2022

rigidity, and synthetic accessibility [10,11]. In the last decade, three drugs containing the DKP scaffold – Tadalafil, Retosiban, and Epelsiban – entered the market for the treatment of male sexual function problems, spontaneous preterm labour, and premature ejaculation in men, respectively [12–14].

It is well-known that the blood-brain barrier (BBB) represents an obstacle to the successful delivery of drugs to the central nervous system (CNS) [15]. In the context of CNS diseases, much medicinal chemistry- or technology-based approaches were explored [16–18]. The DKP-based motif was recently considered as a potential blood-brain barrier shuttle (BBB-shuttle) for the delivery of drugs with limited ability to cross the BBB. Teixido et al. (2007) took advantage of the DKP scaffold to guarantee the passive transport of dopamine and baicalin through the BBB as demonstrated by PAMPA assays [19]. Guan et al. (2009) demonstrated that the DKP NNZ-2591 (cyclo-L-glycyl-L-2 allylproline) improved the long-term recovery in the rat model of Parkinson's Disease (PD) after the onset of motor deficit [20]. In our previous paper, we designed and synthesized a series of potential anti-Parkinson codrugs in which L-Dopa (LD) was linked to cysteine, methionine, and bucillamine [21]. Our findings indicated that N-Acetyl-L-Methionine-L-Dopa-methyl ester, showing a good radical scavenging activity, underwent bioconversion to LD in rat and human plasma thus reducing LD plasma fluctuation (Fig. 1). *In vivo* experiments demonstrated that N-Acetyl-L-Methionine-L-Dopa-methyl ester exerted protective effects against oxidative stress – via Nrf2 activation – leading to ROS decrease and GSH enhancement thus preventing dopaminergic neuronal death [22]. However, the drug-likeness properties of this codrug revealed that it has low gastrointestinal (GI) absorption and no capability of crossing the BBB.

In the framework of our investigations towards the improvement of the GI and BBB-permeation of this molecule, the aim of this work was the development of DKPs – containing the key elements (antioxidant portions and L-Dopa) that were responsible for the biological activity of the above-mentioned codrug – able to reach the diseased brain areas of PD patients. Notably, the catechol group was acetylated compared to the linear peptide to avoid the auto-oxidation process of L-Dopa. In fact, the auto-oxidation of L-Dopa to Dopa quinone leads to the formation of reactive intermediates that are implicated in cellular damage. As antioxidant portions in addition to methionine, we investigated other cysteine derivatives such as free cysteine, S-methyl-, S-ethyl-, S-allyl, and S-propargyl-cysteine. Specifically, this work includes the synthesis of L-Dopa-containing diketopiperazines (**DKP1-6**) and the evaluation of their physicochemical, biological, and genotoxic properties in different *in vitro* models for establishing their possible suitability in pharmaceutical applications (Chart 1). Notably, PC12 cells – treated with the potent neurotoxin MPP^+ responsible for parkinsonian syndrome in experimental models – were used as *in vitro* model to study the anti-Parkinson properties of **DKP1-6**. On the other hand, the genotoxic, oxidative, and cytotoxic effects of **DKP1-6** were investigated in newborn rat cerebral cortex (RCC) and primary human whole blood (PHWB) cell cultures for the first time. The levels of total antioxidant capacity (TAC) and total oxidative stress (TOS) were also determined to assess the oxidative damage potential. Comet assay was used to detect DNA damage and the content of 8-hydroxyl-2′-deoxyguanosine (8-OH-dG), a hallmark of oxidative DNA damage, was quantitatively measured in both cell types. In addition, genotoxic damage potentials of **DKP1-6** were also investigated in PHWB cells using sister chromatid exchange (SCE) and micronuclei (MN) assays. Finally, **DKP1-6** stability studies were performed in simulated gastric and intestinal fluids at pH 1.2 and 7.4 and human plasma while the capability of crossing the biological membranes was assayed by BBB- and Caco-2 permeability assays.

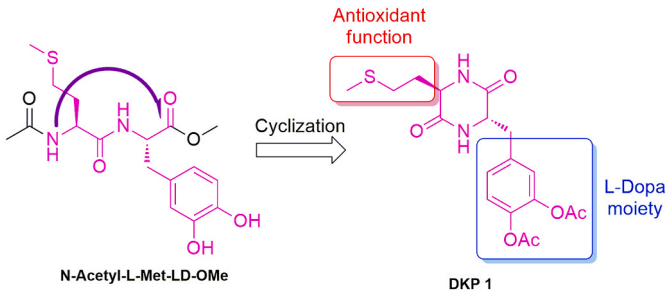

Fig. 1. Design of L-Dopa-containing diketopiperazines.

2. Results and discussion

2.1. Chemistry

The synthesis of **DKP1-6** was successfully achieved following the classical solution synthetic procedures via Boc chemistry (Scheme 1).

Commercially available Boc-derivatives (**1a-f**) were coupled with HCl·H-LD(OAc)$_2$-OMe [23] in the presence of isobutyl chloroformate (IBCF) and Triethylamine (TEA) in DMF to give **2a-f** in good yields (>45%). The treatment of **2a-f** with TFA in dichloromethane – to remove the Boc protecting group – quantitatively provided compounds **3a-f** subsequently used for cyclization. Diketopiperazine scaffold was

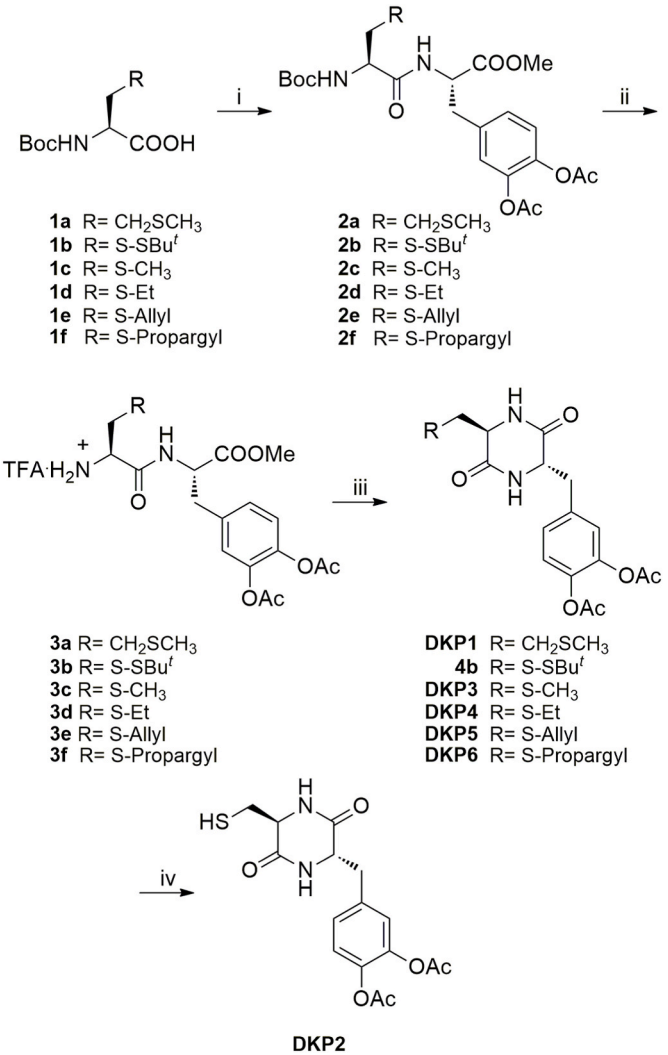

Scheme 1. Synthesis of **DKP1-6**: i) HCl·H-LD(Ac)$_2$-OMe, TEA, IBCF, dry DMF, 20 min, −20 °C, then 2h, 0 °C, and overnight, rt; ii) TFA, dry DCM, 5 h, rt; iii) c) AcOH/2-butanol 0.1 M, NMM, 5 h, 120 °C; iv) (*n*-Bu)$_3$P, MeOH/H$_2$O (2:1), NH$_3$, 75 min, rt.

introduced into the final compounds after reaction of linear trifluoracetate salts **3a-f** in the presence of AcOH/2-butanol and N-methyl-morpholine (NMM) under reflux for 5h. **DKP1**,**3–6** were afforded in good yields (>40%); on the other hand, **DKP2** was obtained after the removal of S-Bu^t by treating compound **4b** with (n-Bu)$_3$P in MeOH/H_2O. **DKP1-6** were fully characterized by NMR and HPLC analysis (NMR spectra and chromatograms are reported in Supporting Information).

2.2. Biological studies

In our approach to designing novel anti-Parkinson agents able to reach the BBB, a DKP scaffold was introduced into the linear sequence of N-Ac-Met-LD-OMe, a promising dipeptide endowed with neuroprotective properties. In this study, the anti-Parkinson properties of **DKP 1–6** were evaluated using PC12 cells, as *in vitro* model of PD, since these cells displayed physiological and comparable characteristics to DA neurons [24]. 1-Methyl-4-phenylpyridinium (MPP^+), the active metabolite of 1-Methyl-4-phenyl-1,2,3,6-tetrahydropyridine, was selected as a potent neurotoxin to induce neurotoxicity in PC12 cells.

MPP^+ causes a parkinsonian syndrome in experimental animals by concentrating in mitochondria, where it leads to ATP depletion and ROS production, thus inducing a highly selective nigrostriatal dopaminergic degeneration [25–27]. By investigating the time- and concentration-dependent effects of MPP^+ on PC12 cells, we found that MPP^+ induced a significant decrease in cell viability at any tested time and concentration with a survival rate of about 60% at 25 μM MPP^+ after a 24 h treatment (data not shown). Next, we evaluated the effects of a 24 h pre-treatment with L-Dopa methyl ester (H-LD-OMe), the most effective medication for controlling PD symptoms, on cell survival after 24 h MPP^+ exposure [28]. Pre-treatment of PC12 cells with 50 μM H-LD-OMe, as expected, abolished the toxic effects of MPP^+ by increasing cell viability to control levels (Fig. 2). Since a long-term treatment with L-Dopa enhances oxidative stress, we decided to test the cytoprotective effects of **DKP1-6**. The presence of sulfur-containing amino acid in the structure of DKP1-6 has earned great attention due to the pivotal role played by intracellular GSH in antioxidant cell defense and in redox regulation [21]. The protective effect of **DKP5-6**, in which the sulfhydryl group was replaced by S-Allyl (**DKP5**) and S-Propargyl (**DKP6**) groups, respectively, resulted detectable on a nanomolar scale and was even more marked than that of **DKP1-2** (micromolar scale) and

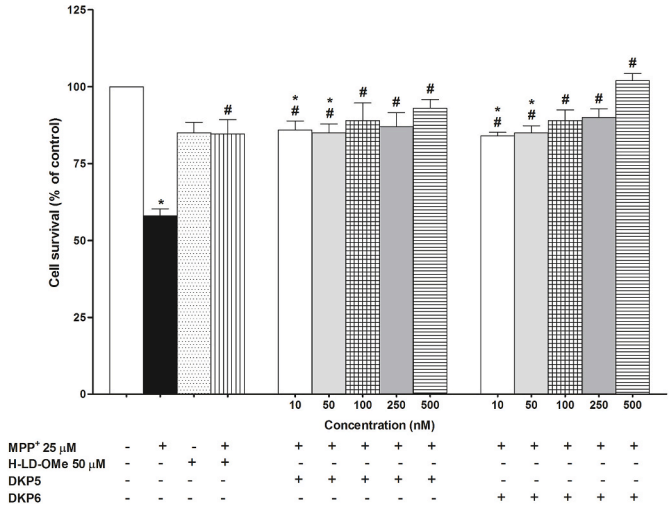

Fig. 2. Cytoprotective effects of **DKP5-6** in PC12 cells exposed to MPP^+. PC12 cells, pre-treated with increasing concentration of **DKP5-6** (10–500 nM) for 24 h, were exposed to MPP^+ (25 μM) for a further 24 h and the cell viability was assessed by MTT test. The absorbance of untreated cells (1.2 ± 0.2) was assumed as 100%. Data represent means ± SD (n = 3). *P < 0.05 vs untreated cells; $^{\#}$P < 0.05 vs MPP $^+$ -treated cells.

DKP3-4 (nanomolar scale) (Figs. 2 and 1S, Supporting information). Thus, **DKP5-6** were chosen to investigate the molecular mechanism underlying the cytoprotective effects on MPP $^+$ -induced cell death. DKPs alone did not modify cell viability (data not shown).

DKP 6 prevents MPP + -induced toxicity by activating Nrf2 nuclear translocation.

Overproduction of ROS and a gradual decline of cellular GSH levels have been proposed as important mechanisms underlying the cytotoxicity of MPP^+ and indicate the MPP^+ possible role to disturb the cellular redox potential and the antioxidant defense systems [29–31]. Therefore, we determined GSH levels and ROS production in PC12 cells exposed to MPP^+. Through a time-course experiment, we found that 25 μM MPP^+ halved GSH levels after a 15–24 h exposure (Fig. 3A). Pre-treatment with 50 μM H-LD-OMe or 100 nM **DKP5** did not prevent MPP $^+$ -induced depletion of cellular GSH, while the addition of 100 nM **DKP6** significantly increased GSH levels (Fig. 3B). Next, we analyzed ROS generation and found that H-LD-OMe and **DKP5-6** were all capable of significantly decreasing MPP $^+$ -induced ROS production (Fig. 3B). It is known that perturbation in ROS and GSH homeostatic levels is sensed by Nrf2, a nuclear factor that is a strong activator of antioxidant responsive element (ARE)-mediated gene expression [24]. We found that the MPP^+ treatment resulted in a moderate Nrf2 nuclear translocation, unaffected by H-LD-OMe, and further increased by **DKP6** pre-treatment (Fig. 3C). Analyses of gene expression by real-time PCR confirmed the activation of the Nrf2-antioxidant response by **DKP6** (Fig. 3D). GSTA-2 and GR expression were moderately down-regulated by MPP^+, while GCLM, Gpx, and x-CT were unaffected. Pre-treatment with **DKP6** significantly up-regulated GCLM, GR, GSTA-2, Gpx, and xCT. H-LD-OMe strongly up-regulated Gpx and x-CT and, to a less extent, GR. Overall, these findings suggest a marked effect of **DKP6** on Nrf2 activation that leads to the expression of genes involved in oxidative stress response thus increasing GSH biosynthesis and ROS buffering.

2.2.1. Biosafety evaluation of *DKP5-6*

DKP5-6, being compounds with the best biological profile, were investigated for their genotoxic, oxidative, and cytotoxic effects in newborn rat cerebral cortex (RCC) and primary human whole blood (PHWB) cell cultures (Figs. 4 and 5). MTT absorbance values were as 44.81 ± 3.71% and 45.33 ± 4.18% of that of untreated controls (control$^-$) when the RCC and PHWB cells were exposed to Mitomycin C (MMC, 10^{-7} M) (control$^+$), respectively, indicating that MMC caused cell death (Fig. 4). Likewise, MMC-induced hematological and neurological damages were clearly evidenced by six- and eight-fold increases in the activity of LDH respectively, compared with the observations of control$^-$ groups (Fig. 5). On the contrary, the cultured primary RCC neurons and PHWB cells exposed to 10–500 nM concentrations of **DKP5-6** did not show any significant alterations in cell viability during 24 h as determined by MTT and LDH assays (Figs. 4 and 5).

The effects of **DKP5-6** on oxidant status in RCC and PHWB cell cultures were evaluated by total antioxidant capacity (TAC) and total oxidative stress (TOS) analysis. As shown in Table 1, the treatments with **DKP5-6** did not alter TAC and TOS levels in both cultured cell types.

DNA damage evaluation was performed by single-cell electrophoresis (SCGE, also known as the Comet test). In the Comet assay, no statistically significant difference in the induction of DNA damage was found between the groups treated with different **DKP5-6** concentrations and the negative control for 24 h (Table 2). However, total DNA damage scores were significantly increased by MMC-intoxication when compared to the untreated group. Likewise, the status of 8-oxo-2-deoxyguanosine (8-OH-dG) in cultured RCC and PHWB cells of control and experimental groups is presented in Table 2. It was observed that MMC (at 10^{-7} M) significantly increased 8-OH-dG concentrations in both cell cultures after 24 h. On the contrary, 8-OH-dG levels did not increase in the cell cultures that were treated with different concentrations of tested DKP.

Finally, to assess whether a mutagenic effect was caused or not by

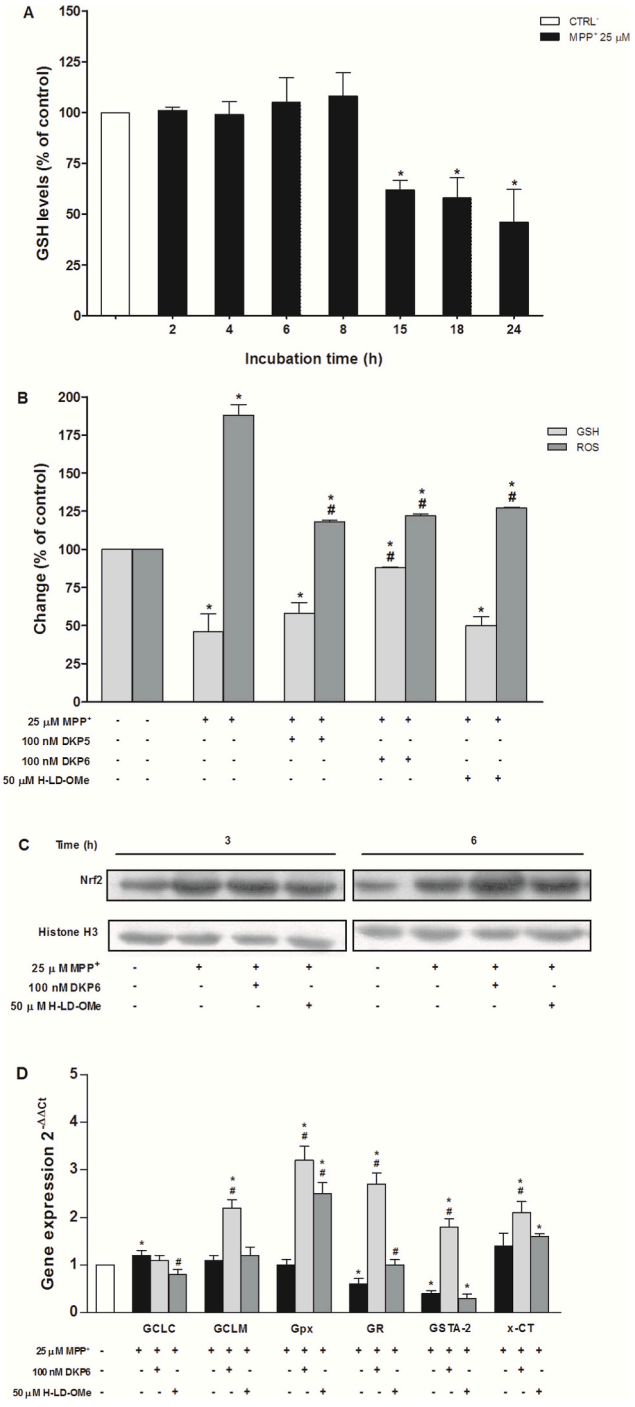

Fig. 3. DKP6 prevents MPP $^{+}$ -induced toxicity by activating Nrf2 nuclear translocation. (A) PC12 cells were incubated with MPP^{+} (25 μM), harvested at the indicated time, and used to assess GSH levels (100% control GSH: 28.35 ± 2.3 nmol/mg protein). (B) Cells were incubated with H-LD-OMe (50 μM) or **DKP5-6** (100 nM) for 24 h prior to treatment with MPP^{+} (25 μM) and then for a further 24 h. GSH levels and ROS generation were detected by DCFH-DA fluorescence (100% control fluorescence: 0.9 ± 0.03). (C) PC12 cells were incubated for 24 h with MPP^{+} (25 μM) either in the absence or in the presence of H-LD-OMe (50 μM) or **DKP6** (100 nM). Nuclear extracts (30 μg) were subjected to Western blotting analysis with the indicated antibodies. Histone H3 was used as a marker for nuclear extracts. (D) PC12 cells were pre-treated for 24h with H-LD-OMe (50 μM) or **DKP6** (100 nM) and exposed to MPP^{+} (25 μM) for 6 h. Changes in gene expression, whose values were normalized to β-Actin, are presented as $2^{-\Delta\Delta}$Ct. Relative mRNA gene abundance in untreated cells was assumed to be 1.0 (control). Data represent means ± SD (n = 3). *P < 0.05 vs. untreated cells; $^{\#}$P < 0.05 vs. MPP $^{+}$ -treated cells.

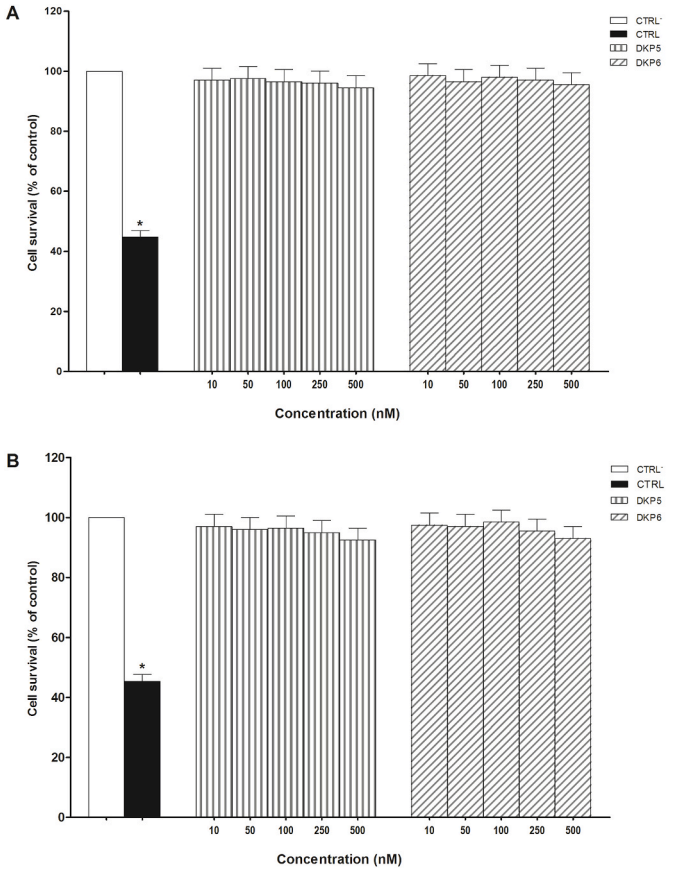

Fig. 4. Cell viability (%) in cultured RCC (Fig. 4A) and PHWB cells (Fig. 4B) treated with **DKP5-6** at the concentrations of 10–500 nM for 24 h and evaluated by MTT assay (values are the means ± standard deviation, $n = 4$, * < 0.05); control^{-}: untreated cells; control: cells treated with MMC at the concentration of 10^{-7} M.

DKP5-6, sister chromatid exchange (SCE) and micronuclei (MN) assays were performed (Table 3). The results of both assays in human lymphocyte cells, following different treatments with **DKP5-6** for 72 h, are presented in Table 3 and Fig. 5S (Supporting Information). As illustrated by our data, SCE and MN analyses did not show statistically significant differences ($p < 0.05$) between untreated cells ($CTRL^{-}$) and any DKP-applied cultures.

2.2.2. *Drug-like physicochemical properties of **DKP5-6***

Drug-like properties, such as solubility, permeability, metabolic stability, and transporter effects are of critical importance for the success of drug candidates [32]. They affect oral bioavailability, metabolism, clearance, toxicity, as well as *in vitro* pharmacology. In this study, drug-like physicochemical properties of the best drug candidates **DKP5-6** were evaluated (Table 4). Both compounds showed low water solubility (<0.7 mg/mL) and lipophilicity, quantified as LogP (<1).

In vitro hydrolysis studies of **DKP5-6** were performed at 37 °C in simulated gastric fluid (hydrochloric acid buffer, pH 1.2), phosphate buffer (pH 7.4), and in the presence of enzymes (pancreatin and pepsin), and human plasma using HPLC with UV detection (Table 5) [33]. It was observed that **DKP6** was more stable both in phosphate buffer (pH 7.4) and in hydrochloric acid buffer (pH 1.2) compared to **DKP5**. Also, in the presence of pepsin, **DKP6** resulted in quite stable showing $t_{1/2}$ higher than 57 h which would guarantee the achievement of the active site after oral administration without undergoing degradation. The observed acid stability of **DKP6** is an essential requirement for oral administration. On the other hand, while **DKP5** underwent rapid hydrolysis in the presence of pancreatin, **DKP6** resulted stable ($t_{1/2}$ > 2.5 h). Moreover, no

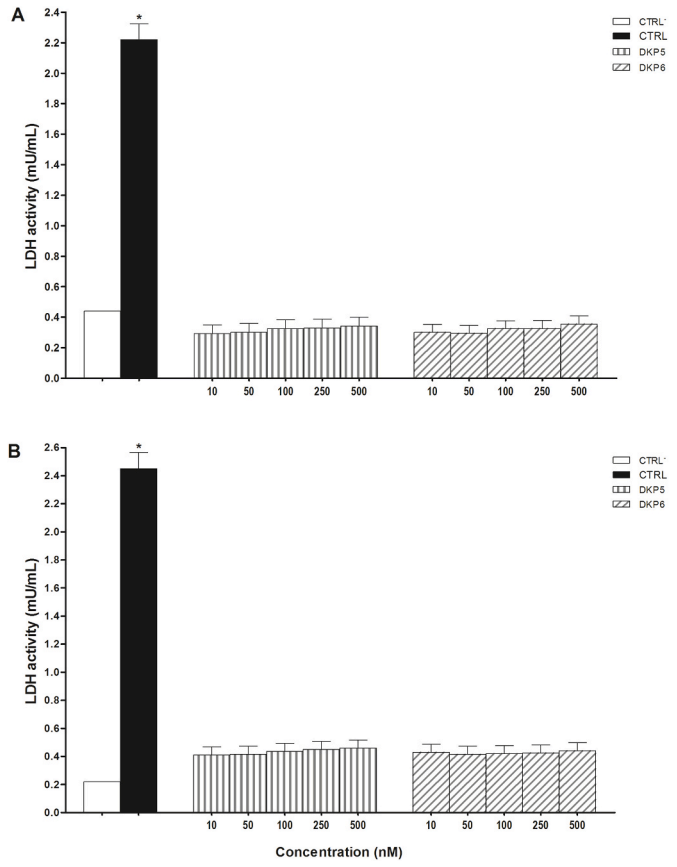

Fig. 5. Extracellular level of LDH in cultured RCC (Fig. 5A) and PHWB cells (Fig. 5B) maintained in the presence of **DKP5-6** at the concentrations of 10–500 nM for 24 h evaluated by LDH assay (values are the means ± standard deviation, $n = 4$, * < 0.05); control^{-}: untreated cells; control: cells treated with MMC at the concentration of 10^{-7} M.

appreciable differences were detected for **DKP6** with respect to its susceptibility to enzymatic hydrolysis in human plasma ($t_{1/2} > 2$ h). These data confirmed that the core DKP scaffold guarantees high stability against the proteolysis of the drug candidate compared to the linear dipeptide [21].

Moreover, the DKP-based motif constitutes a structural requirement for increased cell permeability, higher activity and selectivity, and less cytotoxicity [8]. In this study, to evaluate the increased permeability due to the introduction of the DKP scaffold into the linear sequence of dipeptides, parallel artificial membrane permeability (PAMPA) and

Table 1
The total antioxidant capacity (TAC) and total oxidative stress (TOS) levels in RCC and PHWB cells maintained 24 h in the presence of **DKP5-6** *in vitro*. (Values are means ± standard deviation (n = 4). * <0.05).

Groups		RCC cells		PHWB cells	
		TAC (mmol Trolox equiv/L)	TOS (μmol H_2O_2 equiv/L)	TAC (mmol Trolox equiv/L)	TOS (μmol H_2O_2 equiv/L)
CTRL⁻		14.7 ± 2.8	0.7 ± 0.1	19.3 ± 3.4	0.6 ± 0.1
CTRL		27.5 ± 3.1*	2.3 ± 0.4*	32.5 ± 4.7*	1.9 ± 0.3*
DKP 5	10 nM	15.1 ± 2.5	0.7 ± 0.2	19.2 ± 2.6	0.6 ± 0.1
	50 nM	14.3 ± 2.7	0.7 ± 0.2	19.4 ± 3.2	0.7 ± 0.2
	100 nM	14.4 ± 2.7	0.7 ± 0.1	19.7 ± 2.9	0.7 ± 0.1
	250 nM	14.7 ± 2.9	0.7 ± 0.1	18.8 ± 3.1	0.7 ± 0.1
	500 nM	14.9 ± 2.3	0.7 ± 0.2	18.4 ± 3.3	0.7 ± 0.2
DKP 6	10 nM	14.7 ± 2.6	0.7 ± 0.2	19.4 ± 2.7	0.6 ± 0.1
	50 nM	15.5 ± 2.9	0.6 ± 0.1	19.5 ± 2.9	0.6 ± 0.2
	100 nM	15.2 ± 3.0	0.6 ± 0.1	19.5 ± 2.6	0.6 ± 0.1
	250 nM	15.4 ± 3.1	0.6 ± 0.2	19.8 ± 3.4	0.7 ± 0.1
	500 nM	14.8 ± 2.7	0.6 ± 0.1	19.4 ± 3.0	0.7 ± 0.2

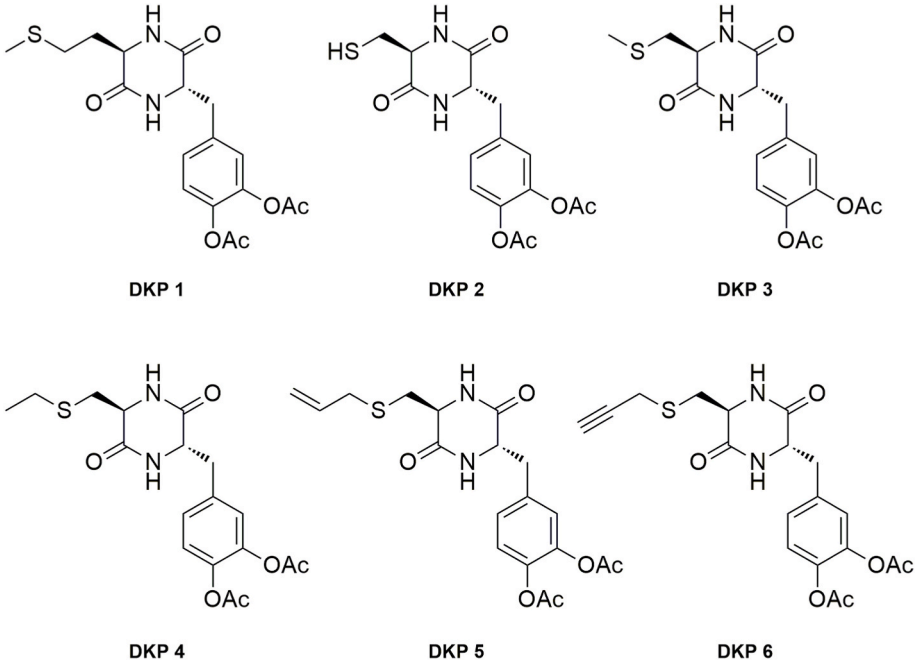

Chart 1. Chemical structures of **DKP1-6**.

Table 2
Comet formations (total DNA damage score) and 8-OH-dG adducts in cultured RCC and PHWB cells were maintained for 24h in the presence of **DKP5-6** *in vitro*. (Values are means ± standard deviation (n = 4). * <0.05).

Groups		RCC cells		PHWB cells	
		Level of 8-OH-dG adducts (as pg/mL)	Total DNA damage score	Level of 8-OH-dG adducts (as pg/mL)	Total DNA damage score
CTRL$^-$		0.14 ± 0.02	36.8 ± 6.3	0.12 ± 0.02	35.4 ± 5.8
CTRL		1.92 ± 0.34*	89.2 ± 7.8*	2.21 ± 0.25*	77.9 ± 8.6*
DKP 5	10 nM	0.14 ± 0.01	36.3 ± 6.7	0.12 ± 0.02	35.0 ± 5.1
	50 nM	0.13 ± 0.03	36.4 ± 4.9	0.12 ± 0.01	35.7 ± 6.0
	100 nM	0.15 ± 0.02	37.1 ± 5.3	0.12 ± 0.02	35.5 ± 5.0
	250 nM	0.15 ± 0.03	37.4 ± 6.9	0.12 ± 0.01	35.7 ± 6.1
	500 nM	0.15 ± 0.02	37.6 ± 6.3	0.13 ± 0.02	36.1 ± 5.3
DKP 6	10 nM	0.14 ± 0.02	36.9 ± 5.5	0.12 ± 0.02	36.0 ± 4.8
	50 nM	0.14 ± 0.02	37.2 ± 5.8	0.11 ± 0.01	35.8 ± 5.5
	100 nM	0.14 ± 0.01	37.8 ± 6.6	0.12 ± 0.02	35.6 ± 7.1
	250 nM	0.14 ± 0.02	37.6 ± 5.9	0.13 ± 0.03	35.9 ± 6.0
	500 nM	0.15 ± 0.02	38.1 ± 6.7	0.13 ± 0.02	36.3 ± 6.2

Table 3
The rates of SCEs and frequencies of CAs and MNs in human lymphocytes treated with different concentrations of **DKP5-6** *in vitro*. Values are means ± standard deviation (n = 4). * <0.05.

Groups		SCEs/cell	MN/1000 cells
CTRL		6.6 ± 0.8	4.5 ± 1.2
CTRL		14.3 ± 1.3*	17.9 ± 2.7*
DKP 5	10 nM	6.8 ± 0.8	4.7 ± 1.0
	50 nM	6.7 ± 0.7	4.9 ± 1.1
	100 nM	6.9 ± 0.7	5.0 ± 0.8
	250 nM	7.1 ± 0.8	5.2 ± 0.8
	500 nM	7.0 ± 1.0	5.2 ± 1.3
DKP 6	10 nM	6.5 ± 0.7	4.6 ± 0.7
	50 nM	6.8 ± 0.5	4.8 ± 0.6
	100 nM	6.6 ± 0.6	4.9 ± 0.9
	250 nM	7.1 ± 0.5	5.1 ± 0.8
	500 nM	6.9 ± 0.8	5.1 ± 1.1

Table 4
Physicochemical properties of **DKP5-6**.

	DKP5	DKP6
Water Solubility (mg/mL)[a]	0.323 (±0.007)	0.63 (±0.02)
LogP[a]	0.68 (±0.02)	0.35 (±0.01)

[a] Values are means of three experiments, standard deviation is given in parentheses.

Caco-2 assays were used.

Notably, the potential CNS passive diffusion properties of **DKP5-6** were evaluated by a cell/free approach such as the PAMPA-BBB assay (Table 6). In agreement with the PAMPA-BBB assay, **DKP6** showed a higher permeability, expressed as Permeability coefficient ($P_e > 4.8 \times 10^{-6}$ cm/s), compared to **DKP5** (*Pe* about 2.4×10^{-6} cm/s) and N-Ac-L-Met-LD-OMe (*Pe* about 1.4×10^{-6} cm/s) suggesting that it could be captured by the BBB through a passive diffusion mechanism. Our results also confirmed the well-known literature data about the reduced capability of LD alone to reach the BBB showing a *Pe* value of about 0.7×10^{-6} cm/s.

To explore additional adsorptive transport mechanisms for **DKP5-6** Caco-2 assays were performed. Results of the Caco-2 test were reported in Table 7 and expressed as permeability coefficient (P_{app}). As suggested by our data, reference compounds were found to be within the low (atenolol) and high (metoprolol and carbamazepine) permeability ranges. Thus, the suitability of the experimental conditions employed was proved. The tested **DKP5** and **DKP6** indicated high permeability compared to the linear dipeptide N-Ac-L-Met-LD-OMe. In agreement with the PAMPA assay (Table 6), **DKP6** shows the highest permeability. In this case, PAMPA and Caco-2 assays seem to have synergistic importance. Since the PAMPA assay estimates the relative passive diffusion rate of drugs, it is likely that, as suggested by the enhanced permeability through the Caco-2 assay, additional adsorptive transport mechanisms can be supposed for the investigated molecules.

In the present study, we demonstrated that **DKP6** containing the S-propargyl moiety in the diketopiperazine scaffold resulted in the most promising drug candidate in terms of physicochemical and biological properties. The presence of the propargyl group guarantees a moderate water solubility compared to the most soluble **DKP4** and **DKP2** (data reported in the SI) and a good LogP value (in the range of 0–3) which is optimal for the penetration of orally administered drugs through the phospholipid biomembrane via passive diffusion. The most stable DKP in simulated gastric fluids resulted in the **DKP4**, containing the S-ethyl-cysteine, showing $t_{1/2}$ higher than 150 h and **DKP6** in intestinal fluids ($t_{1/2} > 3$ h). In human plasma **DKP3**, bearing the S-methyl-cysteine moiety, showed the greatest resistance to the attack of enzymes ($t_{1/2} > 8$ h). PAMPA-BBB assays revealed that only **DKP6** had the capability to pass through the membrane by passive diffusion and so it has been classified as a CNS $^+$ drug. Moreover, the permeability assay performed on Caco-2 cells displayed that **DKP6** was 2.5-fold more permeable than **DKP5** despite its lower lipophilicity suggesting that the S-propargyl-cysteine moiety could interact with the cellular membrane in a different way compared to the S-allyl-cysteine group.

Biological results showed that all **DKP1-6** (in the range of concentrations 10–500 nM) exhibited a percentage of cell survival major that 90% in both cultured RCC and PHWB cells treated with MMC, recognized as a classical DNA damaging agent, on account of its monofunctional and bifunctional DNA alkylating activity [35]. The antioxidant profile was comparable for all DKPs as demonstrated by the determination of TAC and TOS levels in both RCC and PHWB cells. Even if all **DKP1-6** showed no mutagenic effect, only **DKP5-6** – at nanomolar concentrations – displayed a cytoprotective effect (cell viability higher than 80%) in PC12 cells exposed to MPP+, an effective inhibitor of complex I respiration in isolated mitochondria [36]. In the presence of **DKP1-2** – at micromolar concentrations – the cytoprotective effect was reduced to 70% suggesting that the thiol or S-methyl groups were not effective in protecting PC12 cells from the MPP$^+$-induced-neurotoxicity (data reported in the SI).

Notably, even if both **DKP5-6** were able to significantly increase ROS levels in PC12 cells treated with MPP$^+$, only **DKP6** restored GSH levels from 40% to 90% suggesting an indirect involvement in the GSH biosynthesis. Lowered GSH levels and a low GSH/GSSG ratio following oxidative stress are associated with mitochondrial dysfunctions and represent a serious factor in the neurodegeneration that accompanies PD [37]. Our results show that antioxidant approaches associated with a neuroprotective strategy may have therapeutic efficacy in the treatment of PD and its progression.

S-allyl-cysteine and S-propargyl-cysteine – which are responsible for the good biological properties of **DKP5-6** – could be furtherly interesting compared to other sulfur-containing amino acids used in this work for the synthesis of **DKP1-4** due to their function of H_2S donor.

S-allyl-cysteine, the most copious organosulfur compound in aged garlic extract, has several neuroprotective and cardioprotective properties that are exercised possibly via its antioxidant or free radical scavenger action [38]. This sulfur-containing amino acid is considered an endogenous H_2S-producing agent by affording the substrate for

Table 5
Kinetic data for hydrolysis of **DKPs 5–6** at 37 °C.[a]

			DKP 5		DKP 6	
			$t_{½}$ (h)	k_{obs} (h^{-1})	$t_{½}$ (h)	k_{obs} (h^{-1})
Chemical hydrolysis		pH 1.2	18.89 (±0.51)	0.037 (±0.009)	133.5 (±3.1)	0.005 (±0.001)
		pH 7.4	30.93 (±0.71)	0.022 (±0.004)	47.47 (±1.09)	0.015 (±0.003)
Enzymatic hydrolysis	SGF	pepsin 10 mg/mL	24.25 (±0.47)	0.029 (±0.007)	91 (±2.4)	0.008 (±0.002)
		pepsin 40 mg/mL	22.43 (±0.49)	0.031 (±0.007)	57.12 (±1.31)	0.012 (±0.002)
	SIF	pancreatin 10 mg/mL	0.68 (±0.02)	1.03 (±0.02)	3.51 (±0.03)	0.198 (±0.02)
		pancreatin 40 mg/mL	Immediate hydrolysis	–	2.57 (±0.01)	0.270 (±0.03)
Human plasma			0.096 (±0.002)	7.22 (±0.17)	2.09 (±0.01)	0.332 (±0.02)

[a] Values are means of three experiments, standard deviation is given in parentheses.

Table 6
PAMPA-BBB assay of **DKP5-6**.

	Permeability P_e (10^{-6} cm/s)	Classification[a]
L-Dopa	0.75 ± 1.67	CNS^-
DKP 5	2.424 ± 0.49	$CNS^{\pm}$
DKP 6	4.878 ± 0.28	CNS^+
N-Ac-L-Met-LD-OMe	1.424 ± 0.39	CNS^-

[a] CNS^+(indicative of high BBB permeation): P_e (10^{-6} cm/s) > 4.0; $CNS^{+/-}$(discrete BBB permeation): P_e (10^{-6} cm/s) from 4.0 to 2.0. CNS^-(indicative of low BBB permeation): P_e (10^{-6} cm/s) < 2.0.

Table 7
Caco-2 permeability assay of **DKP5-6**.

Compound	Permeability (10^{-6} cm/s)[a] A-B[b]
L-Dopa	0.82 ± 0.23
Atenolol[c]	0.32 ± 6.42
Metoprolol[d]	27.41 ± 5.01
Carbamazepine[d]	50.31 ± 2.19
DKP5	7.50 ± 1.10
DKP6	17.35 ± 2.09
N-Ac-L-Met-LD-OMe	3.50 ± 1.09

[a] Apparent permeability coefficients (P_{app}) were calculated according to equation (1) and data are reported as means ± SD ($n = 3$); values < 5×10^{-6} cm/s, low permeation; values > 5×10^{-6} cm/s, high permeation.
[b] A-B = apical to basolateral direction.
[c] low-permeability marker.
[d] high-permeability markers [34].

cystathionine γ-lyase (CSE) in the H_2S synthesis. On the other hand, S-propargyl-cysteine, which is a structural analog and is more chemically stable than S-allyl-cysteine, showed improved biological properties compared to S-allyl-cysteine such as enhanced plasma H_2S concentrations, increased CSE activity, and anti-cancer and anti-inflammation activity [39,40]. Interestingly, recent evidence reported a link between H_2S and PD [41]. Notably, the endogenous H_2S level in the substantia nigra is significantly decreased in 6-OHDA-treated rats. It was recently observed that supplements of H_2S could weaken the conventional disorders of movement that characterize PD. At the same time, it was found that H_2S protects dopaminergic neurons against MPP^+-induced degeneration in an adenosine triphosphate-sensitive potassium channel–independent, but uncoupling protein 2 (UCP2)–dependent mechanism [42]. These findings suggest that H_2S-based neuroprotective drugs with antioxidant properties against PD, such as **DKP5-6**, could be new hope for the treatment of PD.

3. Conclusion

Cyclic dipeptides represent a class of compounds that can offer many hints for research. In fact, to date among several diketopiperazines found in nature, there are very few of them which have been tested and demonstrated to possess a variety of biological activities. For this purpose, the aim of this work was to synthesize six novel cyclic sulfur-containing amino acid-LD derivatives (**DKP1-6**) combining the antioxidant and neuroprotective activities of the alkylated sulfur-containing residue to L-Dopa, the most used medication for PD. In vitro biological assays on PC12 cells demonstrated that all the six compounds were able to reduce MPP^+-induced toxicity and primarily **DKP5-6** resulted in the most effective compounds even on a nanomolar scale. A further investigation revealed that **DKP6** was capable of significantly increasing GSH levels and counteracting ROS overproduction, even compared to LD-OMe, and preventing MPP^+-induced toxicity by activating Nrf2 nuclear translocation. Moreover, according to the results of a battery of assays performed to evaluate the viability, cytotoxicity, genotoxicity, and oxidative damage in RCC and PHWB cell cultures, the newly synthesized **DKP5-6** could be considered safe for use in pharmaceutical applications, from a toxicological point of view. Permeability assays suggested that **DKP6** could cross the blood-brain barrier via a passive diffusion process representing an exciting challenge for medicinal chemists with the aim of improving the pharmacological efficacy of novel drugs. However, the **DKP6** ability to overcome BBB should be verified using an *in vivo* experimental model of PD. In summary, these encouraging results suggest that the novel synthesized cyclic diketopiperazine **DKP6** could represent a promising H_2S-based neuroprotective candidate with anti-Parkinson and antioxidant properties for the treatment of PD neurodegeneration.

4. Experimental section

4.1. Materials and methods

4.1.1. Chemistry

All the reagents, unless otherwise stated, were from Sigma Aldrich Co. (St. Louis, MO, USA). Compounds **1e-f** were purchased by Aurora Building Block (USA). All other chemicals used were of the highest purity commercially available.

Chromatographic purifications were performed on silica gel using column chromatography (Merck 60, 70–230 mesh ASTM silica gel), and compounds were detected with UV light (λ = 254 nm). The purity of **DKP 1–6** was determined by analytical HPLC using a Waters 600 HPLC pump (Waters Corporation, Milfors, MA, USA) equipped with an X-Bridge BEH130 C-18, 5 μm, 4.6 × 250 mm column with Waters 2996 PDA detector, and as solvent system H_2O/CH_3CN (0.1% TFA) in the form of a linear gradient from 10 to 90% of CH_3CN in 20 min and a flow rate of 1 mL/min. **DKP 1–6** were obtained with purity greater than 95%, determined by analytical HPLC at 254 and 280 nm (HPLC chromatograms are reported in the Supporting Information).

NMR spectra of all compounds were recorded with a Varian VXR-300 MHz spectrometer (Varian Medical Systems, Inc., Palo Alto, CA, USA) (NMR spectra of **DKP1-6** are reported in the Supporting Information). Microanalysis (C, H, N) was performed on a Carlo Erba instrument model E1110. Analyses indicated by the symbols of the elements or functions were within ±0.4% of the theoretical values.

General method for coupling (2a-f). A stirring solution of Boc amino acid (7.32 mmol) in dry DMF (15 mL) was added with TEA (1.02

mL) and IBCF (0.96 mL) and left for 20 min at −20 °C. After the formation of the anhydride, the reaction mixture was added with an ice-cold solution of HCl·H-LD(Ac)$_2$-OMe (7.32 mmol) and TEA (1.02 mL) in dry DMF (10 mL) and left overnight at room temperature. After the removal of the solvent, the residue was washed with $CHCl_3$/$KHSO_4$ 1 N, $NaHCO_3$ ss, and brine; the organic layer was dried over anhydrous Na_2SO_4 and evaporated under vacuum. Chromatographic purification on silica gel with CH_2Cl_2/AcOEt as eluant provided dipeptides **2a-f**.

Boc-Met-LD(Ac)$_2$-OMe (2a). Yield: 53%. R_f = 0.33, CH_2Cl_2/AcOEt (3:1); ^{1}H NMR ($CDCl_3$) δ: 1.41 (9H, s, Boc), 1.82–1.99 (2H, m, Met β-CH_2), 2.04 (3H, s, S–CH_3), 2.26 (6H, s, 2 x Ac), 2.48–2.53 (2H, t, J = 7.3 Hz, Met γ-CH_2), 3.06–3.11 (2H, m, LD β-CH_2), 3.70 (3H, s, OMe), 4.23–4.25 (1H, m, Met α-CH), 4.80–4.86 (1H, m, LD α-CH), 5.28–5.31 (1H, d, J = 7.9 Hz, NH), 6.77–6.79 (1H, d, J = 7.7 Hz, NH), 6.94–7.09 (3H, m, Ar); ^{13}C NMR ($CDCl_3$) δ: 15.38 (S–CH_3), 20.8 (CH_3, Ac), 20.99 (CH_3, Ac), 28.49 (Boc), 30.35 (Met γ-CH_2), 31.60 (Met β-CH_2), 37.36 (LD β-CH_2), 52.77 (Met α-CH), 53.07 (LD α-CH), 53.62 (OMe), 80.29 (Boc, C), 123.70–127.57 (3 x CH Ar), 134.76–142.03 (3 x C Ar), 155.84–171.61 (5 x CO).

Boc-Cys(S-Bu^t)-LD(Ac)$_2$-OMe (2b). Yield: 47%. R_f = 0.70, CH_2Cl_2/AcOEt (4:1); ^{1}H NMR ($CDCl_3$) δ: 1.32 (9H, s, S-Bu^t), 1.44 (9H, s, Boc), 2.27 (6H, s, 2 x Ac), 3.06–3.11 (2H, m, Cys β-CH_2), 3.13–3.20 (2H, m, LD β-CH_2), 3.71 (3H, s, OMe), 4.40–4.44 (1H, m, Cys α-CH), 4.82–4.88 (1H, q, LD α-CH), 5.37–5.39 (1H, d, J = 7.9 Hz, NH), 6.85–6.87 (1H, d, J = 7.8 Hz, NH), 6.99–7.10 (3H, m, Ar); ^{13}C NMR ($CDCl_3$) δ: 20.83 (CH_3, Ac), 20.94 (CH_3, Ac), 28.46 (Boc), 30.10 (S-Bu^t), 33.02 (Cys β-CH_2), 37.36 (LD β-CH_2), 45.52 (S-Bu^t, C), 52.75 (Cys α-CH), 53.31 (LD α-CH), 54.02 (OMe), 79.51 (Boc, C), 123.61–127.55 (3 x CH Ar), 133.98–142.05 (3 x C Ar), 168.47–171.35 (5 x CO).

Boc-Cys(Methyl)-LD(Ac)$_2$-OMe (2c). Yield: 48%. R_f = 0.60, CH_2Cl_2/AcOEt (2:1); ^{1}H NMR ($CDCl_3$) δ: 1.44 (9H, s, Boc), 2.10 (3H, s, S–CH_3), 2.27 (6H, s, 2 x Ac), 2.80–2.82 (2H, d, Cys β-CH_2), 3.04–3.19 (2H, m, LD β-CH_2), 3.71 (3H, s, OMe), 4.21–4.28 (1H, m, Cys α-CH), 4.82–4.88 (1H, m, LD α-CH), 5.41 (1H, d, J = 6.8 Hz, NH), 6.95 (1H, s, NH), 6.98–7.10 (3H, m, Ar); ^{13}C NMR ($CDCl_3$) δ: 16.05 (S–CH_3), 20.88 (CH_3, Ac), 20.99 (CH_3, Ac), 28.48 (Boc), 36.47 (Cys β-CH_2), 37.41 (LD β-CH_2), 52.81 (Cys α-CH), 53.31 (LD α-CH), 53.65 (OMe), 79.51 (Boc, C), 123.67–127.53 (3 x CH Ar), 134.75–142.06 (3 x C Ar), 168.49–171.38 (5 x CO).

Boc-Cys(Ethyl)-LD(Ac)$_2$-OMe (2d). Yield: 49%. R_f = 0.66, CH_2Cl_2/AcOEt (2:1); ^{1}H NMR ($CDCl_3$) δ: 1.18–1.25 (3H, t, S–CH_2CH_3), 1.42 (9H, s, Boc), 2.25 (6H, s, 2 x Ac), 2.49–2.56 (2H, q, S–CH_2CH_3), 2.82–2.84 (2H, m, Cys β-CH_2), 3.02–3.16 (2H, m, LD β-CH_2), 3.68 (3H, s, OMe), 4.23–4.25 (1H, m, Cys α-CH), 4.79–4.86 (1H, q, LD α-CH), 5.42 (1H, d, J = 6.8 Hz, NH), 6.97 (1H, s, NH), 6.99–7.09 (3H, m, Ar); ^{13}C NMR ($CDCl_3$) δ: 14.89 (S–CH_2CH_3), 20.81 (CH_3, Ac), 20.91 (CH_3, Ac), 26.57 (S–CH_2CH_3), 28.45 (Boc), 33.96 (Cys β-CH_2), 37.39 (LD β-CH_2), 52.70 (Cys α-CH), 53.34 (LD α-CH), 54.12 (OMe), 79.51 (Boc, C), 123.59–127.51 (3 x CH Ar), 134.77–142.06 (3 x C Ar), 168.40–171.34 (5 x CO).

Boc-Cys(Allyl)-LD(Ac)$_2$-OMe (2e). Yield: 57%. R_f = 0.73, CH_2Cl_2/AcOEt (2:1); ^{1}H NMR ($CDCl_3$) δ: 1.43 (9H, s, Boc), 2.25 (6H, s, 2 x Ac), 2.77–2.79 (2H, m, Cys β-CH_2), 3.05–3.10 (2H, m, LD β-CH_2), 3.11–3.14 (2H, m, S–CH_2CHCH_2), 3.69 (3H, s, OMe), 4.24–4.26 (1H, m, Cys α-CH), 4.80–4.85 (1H, q, LD α-CH), 5.07–5.16 (2H, m, S–CH_2CHCH_2), 5.37 (1H, d, J = 6.9 Hz, NH), 5.70–5.75 (1H, m, S–CH_2CHCH_2), 6.87–6.89 (1H, d, J = 7.3 Hz, NH), 6.98–7.09 (3H, m, Ar); ^{13}C NMR ($CDCl_3$) δ: 20.83 (CH_3, Ac), 20.94 (CH_3, Ac), 28.46 (Boc), 33.02 (Cys β-CH_2), 35.20 (S–CH_2CHCH_2), 37.36 (LD β-CH_2), 52.75 (Cys α-CH), 53.31 (LD α-CH), 54.02 (OMe), 79.51 (Boc, C), 118.15 (S–CH_2CHCH_2), 123.61–127.55 (3 x CH Ar), 134.76 (S–CH_2CHCH_2), 133.98–142.05 (3 x C Ar), 168.47–171.35 (5 x CO).

Boc-Cys(Propargyl)-LD(Ac)$_2$-OMe (2f). Yield: 65%. R_f = 0.71, CH_2Cl_2/AcOEt (2:1); ^{1}H NMR ($CDCl_3$) δ: 1.42 (9H, s, Boc), 2.26 (6H, s, 2 x Ac), 2.27 (1H, s, S–CH_2CCH), 2.92–3.02 (2H, m, Cys β-CH_2), 3.03–3.11 (2H, m, LD β-CH_2), 3.23–3.24 (2H, m, S–CH_2CCH), 3.67 (3H, s, OMe), 4.31–4.36 (1H, m, Cys α-CH), 4.79–4.85 (1H, q, LD α-CH), 5.43–5.45 (1H, d, J = 6.9 Hz, NH), 6.88–6.91 (1H, d, J = 7.1 Hz, NH), 6.95–7.08 (3H, m, Ar); ^{13}C NMR ($CDCl_3$) δ: 20.81 (CH_3, Ac), 20.91 (CH_3, Ac), 28.44 (Boc), 34.24 (Cys β-CH_2), 37.33 (LD β-CH_2), 37.44 (S–CH_2CCH), 52.74 (Cys α-CH), 53.30 (LD α-CH), 53.76 (OMe), 72.20 (S–CH_2CCH), 80.06 (Boc, C), 80.53 (S–CH_2CCH), 123.63–127.56 (3 x CH Ar), 134.74–142.06 (3 x C Ar), 155.49–171.34 (5 x CO).

General method for cyclization (DKP1, DKP3-6, and 4b). Boc-dipeptide methyl ester **2a-f** (7.24 mmol) was dissolved in dry DCM (7.8 mL) and TFA (11 mL). After 5 h of stirring at room temperature, the solvent was removed under vacuum and the residue was repeatedly treated with Et_2O to give the deprotected dipeptides **3a-f** in quantitative yields.

The trifluoroacetate salt **3a-f** (1.31 mmol) was solubilized in AcOH/*n*-butanol 0.1 M (58 mL) and added with NMM (0.14 mL). The solution was stirred under reflux for 5 h at 120 °C. After evaporation of the solvent, **DKP1**,**3** and **4b** were isolated by crystallization with $CHCl_3$ at 4 °C, whereas compounds **DKP4-6** needed to be chromatographed on silica gel using $CHCl_3$/MeOH as eluant.

4-(((2*S*,5*R*)-5-(2-(methylthio)ethyl)-3,6-dioxopiperazin-2-yl) methyl)-1,2-phenylene diacetate (DKP 1). Yield: 47%. R_f = 0.58, $CHCl_3$/MeOH (9:1); ^{1}H NMR (DMSO-d_6) δ: 1.09–1.43 (2H, m, Met β-CH_2), 1.88 (3H, s, S–CH_3), 2.07–2.10 (2H, t, J = 7.8 Hz, Met γ-CH_2), 2.22 (3H, s, Ac), 2.24 (3H, s, Ac), 2.80–3.15 (2H, m, LD β-CH_2), 3.75–3.77 (1H, m, Met α-CH), 4.18–4.21 (1H, m, LD α-CH), 6.99–7.17 (3H, m, Ar), 8.16 (1H, s, NH), 8.22 (1H, s, NH); ^{13}C NMR (DMSO-d_6) δ: 14.87 (S–CH_3), 20.95 (CH_3, Ac), 21.04 (CH_3, Ac), 28.83 (Met γ-CH_2), 33.33 (Met β-CH_2), 37.73 (LD β-CH_2), 53.17 (Met α-CH), 55.64 (LD α-CH), 123.80–129.04 (3 x CH Ar), 135.58–142.19 (3 x C Ar), 166.87–168.80 (4 x CO). Anal. Calcd for $C_{18}H_{22}N_2O_6$: C, 54.81; H, 5.62; N, 7.10; O, 24.34; S, 8.13. Found: C, 54.90; H, 5.71; N, 7.02; O, 24.20, S, 8,17.

Cyclo [Cys(S-Bu^t)-LD(Ac)$_2$] (4b). Yield: 55%. R_f = 0.58, $CHCl_3$/MeOH (9:1); ^{1}H NMR (DMSO-d_6) δ: 1.23 (9H, s, S-Bu^t), 2.14–2.78 (2H, m, Cys β-CH_2), 2.23 (6H, s, 2 x Ac), 2.88–3.13 (2H, m, LD β-CH_2), 3.95–3.99 (1H, m, Cys α-CH), 4.16–4.22 (1H, m, LD α-CH), 7.01–7.16 (3H, m, Ar), 8.17 (1H, s, NH), 8.29 (1H, s, NH); ^{13}C NMR (DMSO-d_6) δ: 15.98 (S-Bu^t), 25.22 (CH_3, Ac), 25.23 (CH_3, Ac), 33.14 (Cys β-CH_2), 40.09 (LD β-CH_2), 43.34 (Cys α-CH), 49.31 (LD α-CH), 50.69 (S-Bu^t, C), 118.85–123.82 (3 x CH Ar), 130.75–137.23 (3 x C Ar), 161.55–163.73 (4 x CO).

4-(((2*S*,5*S*)-5-((methylthio)methyl)-3,6-dioxopiperazin-2-yl) methyl)-1,2-phenylene diacetate (DKP 3). Yield: 50%. R_f = 0.64, $CHCl_3$/MeOH (9:1); ^{1}H NMR (DMSO-d_6) δ: 3.03 (3H, s, S–CH_3), 2.14–2.52 (2H, m, Cys β-CH_2), 2.23 (6H, s, 2 x Ac), 2.89–3.18 (2H, m, LD β-CH_2), 3.92–3.96 (1H, m, Cys α-CH), 4.16–4.23 (1H, m, LD α-CH), 7.03–7.15 (3H, m, Ar), 8.05 (1H, s, NH), 8.26 (1H, s, NH); ^{13}C NMR (DMSO-d_6) δ: 16.38 (S–CH_3), 20.97 (CH_3, Ac), 21.03 (CH_3, Ac), 38.07 (Cys β-CH_2), 39.31 (LD β-CH_2), 54.90 (Cys α-CH), 55.62 (LD α-CH), 123.78–128.94 (3 x CH Ar), 135.89–142.16 (3 x C Ar), 166.69–168.81 (4 x CO). Anal. Calcd for $C_{17}H_{20}N_2O_6S$: C, 53.67; H, 5.30; N, 7.36; O, 25.23; S, 8.43. Found: C, 53.71; H, 5.31; N, 7.32; O, 25.20, S, 8.46.

4-(((2*S*,5*S*)-5-((ethylthio)methyl)-3,6-dioxopiperazin-2-yl) methyl)-1,2-phenylene diacetate (DKP 4). Yield: 43%. R_f = 0.28, $CHCl_3$/MeOH (9:1); ^{1}H NMR ($CDCl_3$) δ: 1.20–1.25 (3H, t, J = 7.5 Hz, S–CH_2CH_3), 1.98–3.07 (2H, m, Cys β-CH_2), 2.27 (6H, s, 2 x Ac), 2.46–2.53 (2H, q, S–CH_2CH_3), 3.18–3.22 (2H, m, LD β-CH_2), 3.94–3.97 (1H, m, Cys α-CH), 4.28–4.32 (1H, m, LD α-CH), 6.47 (1H, s, NH), 6.64 (1H, s, NH), 7.07–7.17 (3H, m, Ar); ^{13}C NMR ($CDCl_3$) δ: 14.91 (S–CH_2CH_3), 20.85 (CH_3, Ac), 20.86 (CH_3, Ac), 26.34 (S–CH_2CH_3), 36.60 (Cys β-CH_2), 39.90 (LD β-CH_2), 54.08 (Cys α-CH), 56.31 (LD α-CH), 124.09–128.43 (3 x CH Ar), 134.16–142.53 (3 x C Ar), 166.31–168.46 (4 x CO). Anal. Calcd for $C_{18}H_{22}N_2O_6S$: C, 54.81; H, 5.62; N, 7.10; O, 24.34; S, 8.13. Found: C, 54.79; H, 5.67; N, 7.15; O, 24.36; S, 8.03.

4-(((2*S*,5*S*)-5-((allylthio)methyl)-3,6-dioxopiperazin-2-yl)

methyl)-1,2-phenylene diacetate (DKP 5). Yield: 68%. R_f = 0.60, $CHCl_3$/MeOH (9:1); ^{1}H NMR (DMSO-d_6) δ: 2.23 (6H, s, 2 x Ac), 2.17–2.53 (2H, m, Cys β-CH_2), 2.93–2.97 (2H, m, S–CH_2CHCH_2), 2.94–3.16 (2H, m, LD β-CH_2), 3.93–3.96 (1H, m, Cys α-CH), 4.17–4.22 (1H, m, LD α-CH), 4.99–5.11 (2H, m, S–CH_2CHCH_2), 5.61–5.70 (S–CH_2CHCH_2), 7.03–7.15 (3H, m, Ar), 8.03 (1H, s, NH), 8.23 (1H, s, NH); ^{13}C NMR (DMSO-d_6) δ: 20.99 (CH_3, Ac), 21.04 (CH_3, Ac), 34.55 (Cys β-CH_2), 34.84 (S–CH_2CHCH_2), 38.38 (LD β-CH_2), 54.83 (Cys α-CH), 55.65 (LD α-CH), 117.78 (S–CH_2CHCH_2), 123.77–128.83 (3 x CH Ar), 135.16 (S–CH_2CHCH_2), 135.97–142.17 (3 x C Ar), 166.67–168.79 (4 x CO). Anal. Calcd for $C_{19}H_{22}N_2O_6S$: C, 56.15; H, 5.46; N, 6.89; O, 23.62; S, 7.89. Found: C, 56.25; H, 5.49; N, 6.91; O, 23.69; S, 7.66.

4-(((2S,5S)-3,6-dioxo-5-((prop-2-yn-1-ylthio)methyl)piperazin-2-yl)methyl)-1,2-phenylene diacetate (DKP 6). Yield: 50%. R_f = 0.43, $CHCl_3$/MeOH (9:1); ^{1}H NMR (DMSO-d_6) δ: 2.27 (6H, s, 2 x Ac), 2.28 (1H, s, S–CH_2CCH), 2.31–2.72 (2H, m, Cys β-CH_2), 2.95–3.17 (2H, m, LD β-CH_2), 3.11–3.12 (2H, m, S–CH_2CCH), 3.87–3.96 (1H, m, Cys α-CH), 4.19–4.23 (1H, m, LD α-CH), 7.02–7.14 (3H, m, Ar), 8.05 (1H, s, NH), 8.31 (1H, s, NH); ^{13}C NMR (DMSO-d_6) δ: 19.58 (S–CH_2CCH), 20.97 (CH_3, Ac), 21.03 (CH_3, Ac), 35.25 (Cys β-CH_2), 38.12 (LD β-CH_2), 54.52 (Cys α-CH), 55.66 (LD α-CH), 74.09 (S–CH_2CCH), 81.25 (S–CH_2CCH), 123.75–128.90 (3 x CH Ar), 135.84–142.17 (3 x C Ar), 166.57–168.80 (4 x CO). Anal. Calcd for $C_{19}H_{20}N_2O_6S$: C, 56.42; H, 4.98; N, 6.93; O, 23.74; S, 7.93. Found. C, 56.32; H, 4.99; N, 6.89; O, 23.72; S, 8.08.

General method for S-Bu^t removal. Compound **4b** (0.989 mmol) was dissolved in a solution of MeOH/H_2O (2:1) (60 mL) made slightly alkaline (pH 8.5) by adding aqueous ammonia; then (n-Bu)$_3$P (0.29 mL) was added to the solution. The reaction mixture was left under stirring for 75 min at room temperature. After evaporation of the solvent, the crude was chromatographed on silica gel using a gradient scale of $CHCl_3$/MeOH (from 98:2 to 9:1) as eluant leading to **DKP2**.

4-(((2S,5S)-5-(mercaptomethyl)-3,6-dioxopiperazin-2-yl) methyl)-1,2-phenylene diacetate (DKP 2). Yield: 53%. R_f = 0.18, $CHCl_3$/MeOH (9:1); ^{1}H NMR (DMSO-d_6) δ: 1.35–1.84 (1H, m, SH), 1.94–2.38 (2H, m, Cys β-CH_2), 2.68–2.96 (2H, m, LD β-CH_2), 3.81–3.86 (1H, m, Cys α-CH), 4.01–4.12 (1H, m, LD α-CH), 6.38–6.59 (3H, m, Ar), 8.02 (1H, s, NH), 8.05 (1H, s, NH), 8.68 (1H, s, OH), 8.74 (1H, s, OH); ^{13}C NMR (DMSO-d_6) δ: 28.37 (Cys β-CH_2), 38.59 (LD β-CH_2), 56.16 (Cys α-CH), 56.76 (LD α-CH), 115.81–121.63 (3 x CH Ar), 127.47–145.58 (3 x C Ar), 166.16–167.33 (2 x CO). Anal. Calcd for $C_{16}H_{18}N_2O_6S$: C, 52.45; H, 4.95; N, 7.65; O, 26.20; S, 8.75. Found: C, 52.47; H, 4.97; N, 7.68; O, 26.18: S, 8.70.

4.1.2. Cell cultures

Undifferentiated rat adrenal pheochromocytoma PC12 cells, sharing important features with dopaminergic neurons [43], were purchased from ATCC (Manassas, VA). PC12 cells were grown in RPMI 1640 medium supplemented with 5% heat-inactivated fetal calf serum, 10% heat-inactivated horse serum, 4 mM glutamine, 50 U/mL penicillin, and 50 mg/mL streptomycin at 37 °C in a humidified 5% CO_2 environment. The cells were split twice a week. The cells were routinely grown in 20 μg/mL polylysine-coated culture flasks.

4.1.3. PC12 cell growth and viability assays

Live PC12 cells were counted using a hemocytometer and cell viability was measured using the conventional 3-[4,5-dimethylthiazol-2-yl]-2,5-diphenyl tetrazolium bromide (MTT) reduction assay. The dark blue formazan crystals formed in intact cells were solubilized with lysis buffer (10% sodium dodecyl sulfate, 0.01 M HCl) and the absorbance at 550 nm was measured with a microplate reader (Seac, Florence, Italy). To ensure that results were comparable between the cell counting methods, calibration curves for MTT absorbance vs. cell numbers in parallel cultures were constructed. A linear relationship between absorbance vs. cell number was found. Results were expressed as the percentages of reduced MTT, assuming the absorbance of control cells as 100%.

4.1.4. Glutathione determination

PC12 cells (7×10^5), seeded in 6-well plates, were detached, and washed twice with Ca^{+2} -/Mg^{+2} –free PBS. The concentration of glutathione (GSH) was determined in whole-cell lysate after perchloric acid precipitation using the dithionitrobenzoic acid (DTNB) method at 412 nm (molar extinction coefficient 13.6 $mmol^{-1}cm^{-1}$). GSH levels were expressed as a percentage of control.

4.1.5. Measurement of intracellular fluorescence

The 2′,7′-dichlorodihydrofluorescein diacetate (DCFH-DA) method was used to detect the levels of intracellular ROS [44]. DCFH-DA diffuses into cells where it is hydrolyzed by intracellular esterase to polar 2′,7′-dichlorodihydrofluorescein. This non-fluorescent fluorescein analog gets trapped inside the cells and is oxidized by intracellular oxidants to a highly fluorescent, 2′,7′-dichlorofluorescein. The fluorescence intensity is proportional to the number of oxidant species produced by the cells. PC12 cells (3×10^4) seeded in 96-well plates were loaded with DCFH-DA (10 μM) for 30 min at 37 °C. The fluorescence of 2′,7′-dichlorofluorescein was detected at 485 nm excitation and at 535 nm emission, using a microplate reader Titertek Fluoroscan II (Flow Laboratories, McLean, VA, USA). Results, expressed as percentage of the control DCF fluorescence, were normalized to cell viability.

4.1.6. Real-time PCR

Total RNA was isolated with TRIZOL Reagent (Invitrogen Ltd, Paisley, UK) according to the manufacturer's instructions and cDNA was synthesized using iScript cDNA synthesis kit (Bio-Rad Lab, Hercules, CA). Real-time PCR was performed using the iCycler iQ detection system (Bio-Rad) and SYBR Green chemistry. Rat primer sequences, obtained from Invitrogen (Invitrogen Ltd, Paisley, UK) were listed in Table 1S (Supporting Information). SYBR Green RT-PCR amplifications were carried out in a 96-well plate in a 25 μL reaction volume that contained 12.5 μL of 2x iQ™ SYBR® Green SuperMix (Bio-Rad), 400 nM forward and reverse primers, and 5–40 ng of cDNA. In each assay, no-template controls were included, and each sample was run in triplicates. The thermal profile consisted of incubation at 95 °C for 3 min, followed by 40 cycles of denaturation for 10 s at 95 °C and an annealing/extension step of 30 s at 62 °C. The mean of Ct values of the stimulated sample was compared to the untreated control sample. ΔCt is the difference in Ct values derived from the target gene (in each assayed sample) and GAPDH, while ΔΔ Ct represents the difference between the paired samples. The n-fold differential ratio was expressed as $2^{-\Delta\Delta Ct}$.

4.2. Western blotting analyses

PC12 cells were processed with NE-PER® Nuclear and Cytoplasmic Extraction Reagents (Pierce Biotechnology, Rockford, IL) according to the manufacturer's instructions. Extracts (30 μg) were loaded on a 10% SDS-polyacrylamide gel and protein levels were determined by western blotting using Nrf2 (C-20) antibody (1:200) and horseradish peroxidase-conjugated -anti IgG antibody (1:5000). Histone H3 (C-16) (1:200) antibody was used as marker proteins for nuclear extracts. Immunocomplexes were visualized with an enhanced chemiluminescence kit (ECL, Pierce Biotechnology, Rockford, IL).

4.2.1. Cytotoxicity and biosafety assays

Primary rat cerebral cortex (RCC) neuron cultures were prepared using rat fetuses as briefly reported. A total of three newborn Sprague-Dawley rats were used in the study. The rats were decapitated by making a cervical fracture in the cervical midline. Then the cerebral cortex was dissected and removed. The cerebral cortex was placed into 5 ml of Hank's balanced salt solution (HBSS), which had already been placed in a sterile Petri dish and macromerotomy was performed using two lancets. This composition was pulled into a syringe and treated at 37 °C for 25–30 min as HBSS plus Trypsin–EDTA (0.25% trypsin–0.02% EDTA) and chemical decomposition was achieved. 8 μL of DNase type 1

(120 U/mL) was added to this solution, treated for 2 min, and centrifuged (3 min and at 800 rpm). After having thrown away the supernatant, 31.5 mL of neurobasal medium (NBM) and 3.5 mL fetal calf serum (FCS) were added to the residue. The obtained single cell after physical and chemical decomposition stages was divided into 3.5 mL samples in each of ten flasks coated with poly-D-lysine formerly dissolved in phosphate-buffered saline (PBS). The flasks were left in the incubator including 5% CO_2 at 37 °C. The flasks were then changed with a fresh medium of half of their volumes every 3 days until the cells were branched and had reached certain maturity; *in vitro* experiments were performed 8 days later [45]. This study was conducted at the Medical Experimental Research Centre in Atatürk University (Erzurum, Turkey). The Ethical Committee of Atatürk University approved the study protocol for the generation of RCC neuron cultures (B.30.2. ATA.0.23.85-73-2014).

The heparinized blood samples were taken from four healthy volunteers with no history of exposure to toxic agents. Questionnaires were performed on all blood donors to evaluate exposure history, and informed consent forms were signed by each of them. For all the volunteers hematological and biochemical parameters were analyzed and normal ranges of hematologic and blood chemistry indices were detected. Experiments were carried out due to the guidelines of the World Medical Assembly (Declaration of Helsinki). PHWB cultures were set up according to a slight modification of the protocol as previously described [46]. The heparinized blood (0.5 mL) was cultured in 6 mL culture medium (Chromosome Medium B, Biochrom®, Germany) containing 5 μg/L of phytohemagglutinin (Biochrom®).

4.2.2. Treatments

Different aqueous concentrations (10, 50, 100, 250 and 500 nM) of each **DKP1-6** were added to cultures. After the application of compounds, the cultures were incubated for 24h at 37 °C to adjust body conditions (except for SCE and MN tests). Mitomycin C (MMC; $C_{15}H_{18}N_4O_5$; Sigma®, at 10^{-7} M) alone added to the group was considered as a positive control (control$^+$) for all genotoxicity and oxidative DNA damage analysis. In similar, ascorbic acid (10 μM) and hydrogen peroxide (25 μM) added groups were also used as the control$^+$ in TAC and TOS analysis, respectively. Each individual RCC and PHWB culture without **DKP1-6** was studied as a negative control group (control$^-$). The cell viability, oxidative, and DNA damage analyses were performed in totally four independent experiments.

4.3. Evaluation of cell viability

4.3.1. MTT assay

The viability of cells was determined by measuring the formation of formazan from MTT spectrophotometrically using commercially available kits (Cayman Chemical®, USA). At the end of the experiment, the cells were incubated with 0.7 mg/mL MTT (30 min and at 37 °C). After the stage of washing, the blue formazan was extracted from the cells with isopropanol/formic acid (95:5) and photometrically determined at 560 nm. The density of formazan formed in control cells was considered as indicating 100% viability [47,48].

4.3.2. LDH assay

Lactate dehydrogenase (LDH) released from damaged cells in a culture medium was quantified by using an LDH assay kit (Cayman Chemical®, USA). A total of 100 μL of cell medium was used for LDH analysis. Released LDH catalyses the oxidation of lactate to pyruvate with simultaneous reduction of NAD^+ to NADH. The rate of NAD^+ reduction was measured as an increase in absorbance at 490 nm. The rate of NAD^+ reduction was directly proportional to LDH activity in the cell medium [49].

4.3.3. TAC and TOS analyses

After cells were exposed to **DKP1-6** for 24h, the cultures were washed with ice-cold PBS and homogenized with 0.9% normal saline. Following homogenization, intracellular levels of TAC and TOS were determined by commercially available kits (Rel Assay Diagnostics®, Turkey) [50].

4.4. Evaluation of DNA damage

4.4.1. Comet assay

DNA damage evaluation was performed by single cell gel electrophoresis (SCGE also known as Comet test) assay. After the application of coverslips, the slides were allowed to gel at 4 °C for 30–60 min. The slides were immersed in freshly prepared cold lysing solution (2.5 M NaCl, 100 mM Na_2 EDTA, 10 mM Tris, 1% sodium sarcosinate, pH 10.0) with 1% Triton X-100 and 10% DMSO added just before use and refrigerated overnight followed by alkali treatment, electrophoresis (at 1.6 V/cm for 20 min, 300 mA) and neutralization (0.4 M Tris, pH 7.5) stages. The dried slides were then stained with ethidium bromide (20 μg/mL) for 10 min [51]. The whole procedure was carried out in dim light to minimize artifact. DNA damage analysis was performed at a magnification of 1009 using a fluorescence microscope (NiconEclips E6600, Japan) after coding the slides by one observer. A total of 100 cells were screened per slide. A total damage score for each slide was derived by multiplying the number of cells assigned to each grade of damage by the numeric value of the grade and summing over all grades (giving a maximum possible score of 500, corresponding to 100 cells at grade 5) [52].

4.4.2. Nucleic acid oxidation

8-Hydroxy-2'-deoxyguanosine assay kits were purchased from Cayman Chemical® for determining 8-OH-dG levels in the cultures. All procedures were carried out in accordance with the provider manual [53].

4.4.3. Sister chromatid exchange assay

For successive visualization of sister chromatid exchange (SCEs), 5-bromo-2-deoxyuridine (Sigma®) was added at culture initiation. The blood cultures were incubated in complete darkness for 72h at 37 °C. Exactly 70h and 30 min after beginning the incubations, demecolcine (N-Deacetyl-N-methylcolchicine, Sigma®) was added to the cultures. After hypotonic treatment (0.075 M KCl), followed by three repetitive cycles of fixation in methanol/acetic acid solution (3:1, v/v), centrifugation, and resuspension, the cell suspension was dropped onto cold microscopic slides, air-dried, aged for 3 days, and then differentially stained for the inspection of the SCE rate according to fluorescence plus Giemsa (FPG) procedure. For each treatment condition, well-spread 30-s division metaphases containing 42–46 chromosomes in each lymphocyte cell were scored by one observer, and the values obtained were presented as SCEs per cell [54].

4.4.4. Micronucleus assay

The Micronucleus assay (MN) test was performed by adding cytochalasin B (Sigma®) after 44h of culture. At the end of the incubation period (72h), the lymphocytes were fixed with ice-cold methanol/acetic acid (1:1, v/v). The fixed cells were placed directly on slides using a cytospin and stained with Giemsa. At least 1000 binucleated lymphocytes were examined per concentration for the presence of one, two or more MN by one observer.

4.4.5. Solubility and lipophilicity

Solubility and LogP were determined as previously reported. HPLC-UV assays were performed using the same methods reported in the chemistry section.

4.4.6. Stability in gastrointestinal fluids

The simulated gastric and intestinal fluids (SGF and SIF respectively) were prepared according to USP specifications. The drug stock solutions

were added to preheated SGF and SIF and placed in a 37 °C shaking water bath. At predetermined time points – (0, 15, 30, and 60 min for SGF and 0, 60, 120, and 180 min for SIF), – 100 μL was deproteinized with 100 μL of ice-cold acetonitrile containing 0.5% v/v of formic acid and placed into micro-centrifuge tubes. The samples were centrifuged at 4 °C and 12,000 rpm for 10 min. The supernatant was filtered and analyzed by HPLC [55].

4.4.7. Human plasma stability

Human plasma was purchased from 3H Biomedical (Uppsala, Sweden, Europe). Enzymatic hydrolysis was evaluated by adding the stock drug solution to a pre-heated (37 °C) plasma fraction, previously diluted with 0.02 M phosphate buffer (pH 7.4) to give a final volume of 1 mL (80% plasma). Samples of 100 μL were taken at various times, and 200 μL of 0.01 M HCl in methanol was used to stop the enzymatic activity. After centrifugation for 5 min at 5000 g, the supernatant was analyzed by HPLC [56].

4.4.8. PAMPA-BBB assay

PAMPA method was used to predict the BBB permeability. The donor solution consisted of a **DKP5-6** stock solution diluted with PBS (pH 7.4) and MeOH (20% v/v) to a final drug concentration of 500 μM. The addition of MeOH as a co-solvent did not affect the properties and composition of lipids [57]. The acceptor solution had the same composition as the donor but without the investigated drugs. The addition of MeOH as a co-solvent was required to guarantee the full solubilization of DKPs in the buffer medium.

The system was assembled by setting 200 μL of the donor and acceptor solutions between an artificial membrane previously coated with a solution (5 μL) of phospholipid mixture derived from porcine polar brain lipid extract. The lipid composition included phosphatidylcholine 12.6%, phosphatidylethanolamine 33.1%, phosphatidylserine 18.5%, phosphatidylinositol 4.1%, phosphatidic acid 0.8%, and 30.9% of other compounds (Avantis Polar Lipids, Alabaster, AL, USA). The resulting system was incubated for 18 h. Concentrations in each donor and acceptor well were determined by HPLC and the effective permeability coefficient (Pe, cm/s) was calculated as previously reported [58].

4.4.9. Caco-2 permeability assay

Hank's balanced salt solution (HBSS), HEPES (25 mM), and Tween 80 (0.1% w/v) were used for the Assay Buffer preparation. The pH of the buffer solution was 6.8. Stock solutions of **DKP5-6** and reference compounds (atenolol, metoprolol, and carbamazepine) were prepared in the assay buffer at a concentration of 125 μg/mL. The Caco-2 cell line was obtained from the European Collection of Authenticated Cell Cultures (ECACC). Cells were seeded at 2.6 cells/cm^2 and grown in a medium comprised of Dulbecco's Modified Eagle's Medium (DMEM) containing 4.5 g/L glucose and supplemented with 10% (v/v) fetal bovine serum (FBS), 1% (v/v) glutamine, penicillin (100 U/mL), streptomycin (100 mg/mL), and 1% Minimum Essential Medium (MEM) nonessential amino acids. Cultures were maintained at 37 °C in an atmosphere of 95% relative humidity and 5% CO_2. The medium was changed every 2–3 days. Routine passing of cell stocks was carried out in 75-cm^2 flasks. All the cells used in this study were between passages 25 and 26.

The TEER of the cell monolayers was measured over a 22-day period. Cells were seeded at 2.6 cells/cm^2 on 1.12 cm^2 polycarbonate membranes with a pore size of 0.4 μm. The TEER measurements were conducted on days 7, 14, 20, and 22 using the EVOM3 instrument (World Precision Instruments, Sarasota, FL, USA). The intrinsic resistance of the system (insert alone) was subtracted from the total resistance (cell monolayer plus insert) to yield the monolayer resistance. The resistance was expressed as Ω x cm^2.

After 4 days of culture, Caco-2 cells reached 100% of confluence and could be spitted for the next passages (Fig. S1). Moreover, in Fig. S2 TEER values of Caco-2 cell monolayers were reported. Measurements were performed during the experimental preparation time (22 days). High levels of TEER suggest Caco-2 cell monolayer integrity.

All transport studies were performed at 37 °C, in HBSS-25 mM HEPES-0.1% Tween 80 buffer. Prior to the permeability studies, cell monolayers were washed with the transport buffer and preincubated for 20 min 500 μL of the test compounds (125 μg/mL), prepared in the Assay Buffer, were added to the apical compartment. All transport studies were carried out in the apical (A) to basolateral (B) direction over a period of 3 h. At fixed time points, ranging from 0 to 180 min, 500 μL of samples were collected from the basolateral chambers for analysis and replaced by an equal volume of fresh buffer. The donor solution was sampled at the beginning (10 μL) and at the end (150 μL) of the experiment to assess the initial and final concentration of the compounds, respectively. All the samples were analyzed using the HPLC instrument and the conditions reported in the chemistry section.

Permeability was estimated by calculating the apparent permeability coefficient (P_{app}) according to the following formula:

$$Papp = J/A_sC_0 \ (\mathrm{cm \bullet s^{-1}}) \quad (1)$$

where J is the initial flux of the drug, determined from the slope of the linear plot of the cumulative amount of drug transported *versus* time, C_0 is the initial concentration in the donor compartment, and A_s is the area of the cell monolayer [59,60].

4.5. Statistical analysis

The data are expressed as the mean ± standard derivation (SD) of four repetitions. One-way analysis of variance (ANOVA) was used to determine the significant differences between the groups followed by a Dunnett's *t*-test for multiple comparisons. A probability <0.05 was considered as significant. All analyses were performed using SPSS version 15.0 (SPSS Inc®, USA).

Author contributions

The manuscript was written through the contributions of all authors. All authors have given approval to the final version of the manuscript.

Funding sources

This research project was supported by the Italian Ministry of Education, University and Research (University "G. d'Annunzio" of Chieti-Pescara) FAR 2020.

Declaration of competing interest

The authors declare that they have no known competing financial interests or personal relationships that could have appeared to influence the work reported in this paper.

Data availability

I have share the link to my data at the attached file

Appendix A. Supplementary data

Supplementary data to this article can be found online at https://doi.org/10.1016/j.ejmech.2022.114746.

References

[1] K.L. Zhao, R.R. Xing, X.H. Yan, Cyclic dipeptides: biological activities and self-assembled materials, Pept. Sci. 113 (2021), e24202, https://doi.org/10.1002/pep2.24202.
[2] Z. Song, Y. Hou, Q. Yang, X. Li, S. Wu, Structures and biological activities of diketopiperazines from marine organisms: a Review, Mar. Drugs 19 (2021) 403, https://doi.org/10.3390/md19080403.

[3] M.B. Martins, I. Carvalho, Diketopiperazines: biological activity and synthesis, Tetrahedron 63 (2007) 9923–9932, https://doi.org/10.1016/j.tet.2007.04.105.

[4] C. Winyakul, W. Phutdhawong, P. Tamdee, J. Sirirak, T. Taechowisan, W. S. Phutdhawong, 2,5-diketopiperazine derivatives as potential anti-influenza (H5N2) agents: synthesis, biological evaluation, and molecular docking study, Molecules 27 (2022). https://doi:10.3390/molecules27134200.

[5] H. Turkez, I. Cacciatore, M.E. Arslan, E. Fornasari, L. Marinelli, A. Di Stefano, A. Mardinoglu, Histidyl-proline diketopiperazine isomers as multipotent anti-alzheimer drug candidates, Biomolecules 10 (2020) 737, https://doi.org/10.3390/biom10050737.

[6] Z.P. Ding, F.F. Li, C.J. Zhong, F. Li, Y.Q. Liu, S.X. Wang, J.C. Zhao, W.B. Li, Structure-based design and synthesis of novel furan-diketopiperazine-type derivatives as potent microtubule inhibitors for treating cancer, Bioorg. Med. Chem. 28 (2020), 115435, https://doi.org/10.1016/j.bmc.2020.115435.

[7] D. Gang, D.W. Kim, H.S. Park, Cyclic peptides: promising scaffolds for biopharmaceuticals, Genes 9 (2018) 557, https://doi.org/10.3390/genes9110557.

[8] L. Feni, L. Jutten, S. Parente, U. Piarulli, I. Neundorf, D. Dia, Cell-penetrating peptides containing 2,5-DKP scaffolds as shuttles for anti-cancer drugs: conformational studies and biological activities, Chem. Commun. 56 (2020) 5685–5688, https://doi.org/10.1039/D0CC01490G.

[9] C. Cornacchia, I. Cacciatore, L. Baldassarre, A. Mollica, F. Feliciani, F. Pinnen, 2,5-Diketopiperazines as neuroprotective agents, Mini-Rev. Med. Chem. 12 (2012) 2–12, https://doi.org/10.2174/138955712798868959.

[10] A.D. Borthwick, 2.5-Diketopiperazines: synthesis, reactions, medicinal chemistry, and bioactive natural products, Chem. Rev. 112 (2012) 3641–3716, https://doi.org/10.1021/cr200398y.

[11] A.S.M. Delatouche, R. Gennari, C. Piarulli, Bifunctional 2,5-diketopiperazines as rigid three-dimensional scaffolds in receptors and peptidomimetics, Eur. J. Org. Chem. 2 (2011) 217–228, https://doi.org/10.1002/ejoc.201001330.

[12] A. Daugan, P. Grondin, C. Ruault, A.C. Le Monnier de Gouville, H. Coste, J. M. Linget, J. Kirilovsky, F. Hyafil, R. Labaudinière, The discovery of tadalafil: a novel and highly selective PDE5 inhibitor. 2: 2,3,6,7,12,12a-hexahydropyrazino [1′,2′:1,6]pyrido[3,4-b]indole-1,4-dione analogues, J. Med. Chem. 46 (2003) 4533–4542, https://doi.org/10.1021/jm0300577.

[13] J. Liddle, M.J. Allen, A.D. Borthwick, D.P. Brooks, D.E. Davies, R.M. Edwards, A. M. Exall, C. Hamlett, W.R. Irving, A.M. Mason, The discovery of GSK221149A: a potent and selective oxytocin antagonist, Bioorg. Med. Chem. Lett. 18 (2008) 90–94, https://doi.org/10.1016/j.bmcl.2007.11.008.

[14] A.D. Borthwick, J. Liddle, D.E. Davies, A.M. Exall, C. Hamlett, D.M. Hickey, A. M. Mason, I.E. Smith, F. Nerozzi, S. Peace, Pyridyl-2,5-diketopiperazines as potent, selective, and orally bioavailable oxytocin antagonists: synthesis, pharmacokinetics, and in vivo potency, J. Med. Chem. 26 (2012) 783–796, https://doi.org/10.1021/jm201287w.

[15] Y. Persidsky, S.H. Ramirez, J. Haorah, G.D. Kanmogne, Blood-brain barrier: structural components and function under physiologic and pathologic conditions, J. Neuroimmune Pharmacol. 1 (2006) 223–236, https://doi.org/10.1007/s11481-006-9025-3.

[16] P. Vlieghe, M. Khrestchatisky, Medicinal chemistry-based approaches and nanotechnology-based systems to improve CNS drug targeting and delivery, Med. Res. Rev. 33 (2013) 457–516, https://doi.org/10.1002/med.21252.

[17] R. Pandit, L. Chen, J. Götz, The blood-brain barrier: physiology and strategies for drug delivery, Adv. Drug Deliv. Rev. 165–166 (2020) 1–14, https://doi.org/10.1016/j.addr.2019.11.009.

[18] S. Cunha, M.H. Amaral, J.M. Sousa Lobo, A.C. Silva, Therapeutic strategies for Alzheimer's and Parkinson's diseases by means of drug delivery systems, Curr. Med. Chem. 23 (2016) 3618–3631, https://doi.org/10.2174/0929867323666160824162401.

[19] M. Teixidó, E. Zurita, M. Malakoutikhah, T. Tarragó, E. Giralt, Diketopiperazines as a tool for the study of transport across the blood-brain barrier (BBB) and their potential use as BBB-shuttles, J. Am. Chem. Soc. 129 (2007) 11802–11813, https://doi.org/10.1021/ja073522o.

[20] R.V.M. Krishnamurthi, S. Mathai, A.H. Kim, R. Zhang, J. Guan, A novel diketopiperazine improves functional recovery given after the onset of 6-OHDA-induced motor deficit in rats, Br. J. Pharmacol. 156 (2009) 662–672, https://doi.org/10.1111/j.1476-5381.2008.00064.x.

[21] F. Pinnen, I. Cacciatore, C. Cornacchia, P. Sozio, L.S. Cerasa, A. Iannitelli, A. Di Stefano, Codrugs linking L-dopa and sulfur-containing antioxidants: new pharmacological tools against Parkinson's disease, J. Med. Chem. 52 (2009) 559–563, https://doi.org/10.1021/jm801266x.

[22] A. Minelli, C. Conte, E. Prudenzi, I. Cacciatore, C. Cornacchia, E. Taha, F. Pinnen, N-acetyl-L-methionyl-L-dopa-methyl ester as a dual-acting drug that relieves L-dopa-induced oxidative toxicity, Free Radic. Biol. Med. 49 (2010) 31–39, https://doi.org/10.1016/j.freeradbiomed.2010.03.011.

[23] J. Leppänen, J. Huuskonen, T. Nevalainen, J. Gynther, H. Taipale, T. Järvinen, Design and synthesis of a novel L-dopa - entacapone codrug, J. Med. Chem. 45 (2002) 1379–1382, https://doi.org/10.1021/jm010980d.

[24] D.A. Zachor, J.F. Moore, C. Brezausek, A. Theibert, A.K. Percy, Cocaine inhibits NGF-induced PC12 cells differentiation through D1-type dopamine receptors, Brain Res. 869 (2000) 85–97, https://doi.org/10.1016/S0006-8993(00)02355-6.

[25] W. Choi, S.E. Kruse, R.D. Palmiter, Z. Xia, Mitochondrial complex I inhibition is not required for dopaminergic neuron death induced by rotenone, MPP+, or paraquat, Proc. Natl. Acad. Sci. USA 105 (2008) 15136–15141, https://doi.org/10.1073/pnas.0807581105.

[26] W. Dauer, S. Przedborski, Parkinson's disease: mechanisms and models, Neuron 39 (2003) 889–909, https://doi.org/10.1016/S0896-6273(03)00568-3.

[27] R. Ying, H.L. Liang, H.T. Whelan, J.T. Eells, M.T. Wong-Riley, Pre-treatment with near-infrared light via light-emitting diode provides added benefit against rotenone- and MPP+-induced neurotoxicity, Brain Res. 1243 (2008) 167–173.

[28] T. Nagatsua, M. Sawadab, L-dopa therapy for Parkinson's disease: past, present, and future, Park. Relat. Disord. 15 (2009), https://doi.org/10.1016/S1353-8020(09)70004-5. S3-S8.

[29] S. Bharath, B.C. Cochran, M. Hsu, J. Liu, B.N. Ames, J.K. Andersen, Pre-treatment with R-lipoic acid alleviates the effects of GSH depletion in PC12 cells: implications for Parkinson's disease therapy, Neurotoxicology (Little Rock) 23 (2002) 479–486, https://doi.org/10.1016/S0161-813X(02)00035-9.

[30] M. Smeyne, R.J. Smeynen, Glutathione metabolism and Parkinson's disease, Free Radic. Biol. Med. 62 (2013) 13–25, https://doi.org/10.1016/j.freeradbiomed.2013.05.001.

[31] K. Wimalasena, Current status, gaps, and weaknesses of the mechanism of selective dopaminergic toxicity of MPTP/MPP^+, Adv. Mol. Toxicol. 11 (2017) 81–122, https://doi.org/10.1016/B978-0-12-812522-9.00003-8.

[32] C. Jia, J.- Li, G.- Hao, G. Yang, A drug-likeness toolbox facilitates ADMET study in drug discovery, Drug Discov, Today Off. 25 (2020) 248–258, https://doi.org/10.1016/j.drudis.2019.10.014.

[33] L. Marinelli, E. Fornasari, P. Eusepi, M. Ciulla, S. Genovese, F. Epifano, I. Cacciatore, Carvacrol prodrugs as novel antimicrobial agents, Eur. J. Med. Chem. 178 (2019) 515–529, https://doi.org/10.1016/j.ejmech.2019.05.093.

[34] D.A. Volpe, J. Patrick, P.J. Faustino, B. Anthony, A.B. Ciavarella, B. Ebenezer, E. B. Asafu-Adjaye, D. Christopher, C.D. Ellison, X. Lawrence, Classification of drug permeability with a Caco-2 cell monolayer assay, Clin. Res. Regul. Aff. 24 (2007) 39–47, https://doi.org/10.1080/10601330701273669.

[35] A. Basu, S. Broyde, S. Iwai, C. Kisker, DNA damage, mutagenesis, and DNA repair, J. Nucleic Acids (2010), https://doi.org/10.4061/2010/182894.

[36] E. Albi, S. Cataldi, M. Codini, G. Mariucci, A. Lazzarini, M.R. Ceccarini, I. Ferri, M. E. Laurenti, C. Arcuri, F. Patria, T. Beccari, C. Conte, Neutral sphingomyelinase increases and delocalizes in the absence of toll-like receptor 4: a new insight for MPTP neurotoxicity, Prostag. Other Lipid Mediat. 142 (2019) 46–52, https://doi.org/10.1016/j.prostaglandins.2019.03.004.

[37] G. Bjørklund, M. Peana, M. Maes, M. Dadar, B. Severin, The glutathione system in Parkinson's disease and its progression, Neurosci. Biobehav. Rev. 120 (2021) 470–478, https://doi.org/10.1016/j.neubiorev.2020.10.004.

[38] X. Cao, L. Cao, L. Ding, J.S. Bian, A new hope for a devastating disease: hydrogen sulfide in Parkinson's Disease, Mol. Neurobiol. 55 (2018) 3789–3799, https://doi.org/10.1007/s12035-017-0617-0.

[39] M. Wang, W. Tang, H. Xin, Y.Z. Zhu, S. Propargyl-Cysteine, A novel hydrogen sulfide donor, inhibits inflammatory hepcidin and relieves anemia of inflammation by inhibiting IL-6/STAT3 pathway, PLoS One 11 (2016), e0163289, https://doi.org/10.1371/journal.pone.0163289.

[40] Q.H. Gong, Q. Wang, L.L. Pan, X.H. Liu, H. Xin, Y.Z. Zhu, S-propargyl-cysteine, a novel hydrogen sulfide-modulated agent, attenuates lipopolysaccharide-induced spatial learning and memory impairment: involvement of TNF signaling and NF-κB pathway in rats, Brain Behav. Immun. 25 (2011) 110–119, https://doi.org/10.1016/j.bbi.2010.09.001.

[41] W. Jiang, W. Zou, M. Hu, Q. Tian, F. Xiao, M. Li, J. Jiang, Hydrogen sulphide attenuates neuronal apoptosis of substantia nigra by re-establishing autophagic flux via promoting leptin signalling in a 6-hydroxydopamine rat model of Parkinson's disease, Clin. Exp. Pharmacol. Physiol. 49 (2022) 122–133, https://doi.org/10.1111/1440-1681.13587.

[42] M. Lu, F.F. Zhao, J.J. Tang, C.J. Su, Y. Fan, J.H. Ding, J.S. Bian, G. Hu, The neuroprotection of hydrogen sulfide against MPTP-induced dopaminergic neuron degeneration involves uncoupling protein 2 rather than ATP-sensitive potassium channels, Antioxidants Redox Signal. 17 (2012) 849–859, https://doi.org/10.1089/ars.2011.4507.

[43] N. Yamamoto, Y. Fukata, M. Fukata, K. Yanagisawa, GM1-ganglioside-induced Aβ assembly on synaptic membranes of cultured neurons, Biochim. Biophys. Acta 1768 (2007) 1128–1137, https://doi.org/10.1016/j.bbamem.2007.01.009.

[44] E. Eruslanov, S. Kusmartsev, Identification of ROS using oxidized DCFDA and flow-cytometry, Methods Mol. Biol. 594 (2010) 57–72, https://doi.org/10.1007/978-1-60761-411-1_4.

[45] H. Turkez, B. Togar, A. Di Stefano, N. Taspınar, P. Sozio, Protective effects of cyclosativene on H_2O_2-induced injury in cultured rat primary cerebral cortex cells, Cytotechnology 67 (2015) 299–309, https://doi.org/10.1007/s10616-013-9685-9.

[46] I. Cacciatore, E. Fornasari, L. Marinelli, P. Eusepi, M. Ciulla, O. Ozdemir, A. Tatar, H. Turkez, A. Di Stefano, Memantine-derived drugs as potential antitumor agents for the treatment of glioblastoma, Eur. J. Pharmaceut. Sci. 109 (2017) 402–411, https://doi.org/10.1016/j.ejps.2017.08.030.

[47] E. Dirican, H. Turkez, In vitro studies on protective effect of glycyrrhiza glabra root extracts against cadmium-induced genetic and oxidative damage in human lymphocytes, Cytotechnology 66 (2014) 9–16, https://doi.org/10.1007/s10616-012-9531-5.

[48] B. Togar, H. Türkez, A. Di Stefano, Zingiberene attenuates hydrogen peroxide-induced toxicity in neuronal cells, Hum. Exp. Toxicol. 34 (2015) 135–144, https://doi.org/10.1177/0960327114538987.

[49] H. Turkez, P. Sozio, F. Geyikoglu, Neuroprotective effects of farnesene against hydrogen peroxide-induced neurotoxicity in vitro, Cell. Mol. Neurobiol. 34 (2014) 101–111, https://doi.org/10.1007/s10571-013-9991-y.

[50] H. Türkez, B. Toğar, Olive (Olea europaea L.) leaf extract counteracts genotoxicity and oxidative stress of permethrin in human lymphocytes, J. Toxicol. Sci. 36 (2011) 531–537, https://doi.org/10.2131/jts.36.531.

[51] J.M. Hartley, V.J. Spanswick, J.A. Hartley, Measurement of DNA damage in individual cells using the single cell gel electrophoresis (Comet) assay, in: I. Cree

(Ed.), Cancer Cell Culture. Methods in Molecular Biology, 731, Humana Press, 2011, https://doi.org/10.1007/978-1-61779-080-5_25.
[52] H. Türkez, K. Çelik, B. Toğar, Effects of copaene, a tricyclic sesquiterpene, on human lymphocytes cells in vitro, Cytotechnology 66 (2014) 597–603, https://doi.org/10.1007/s10616-013-9611-1.
[53] B.A. Abdel-Waha, M.E. Metwally, Ginkgo biloba enhances the anticonvulsant and neuroprotective effects of sodium valproate against kainic acid-induced seizures in mice, J. Pharmacol. Toxicol. 6 (2011) 679–690, https://doi.org/10.3923/jpt.2011.679.690.
[54] E. Dirican, H. Turkez, B. Toğar, Modulatory effects of Thymbra spicata L. different extracts against the mercury-induced genotoxicity in human lymphocytes in vitro, Cytotechnology 64 (2021) 181–186, https://doi.org/10.1007/s10616-011-9406-1.
[55] C. Barbaraci, G. Giurdanella, C.G. Leotta, A. Longo, E. Amata, M. Dichiara, A. Marrazzo, Haloperidol metabolite II valproate ester (S)-(−)-MRJF22: preliminary studies as a potential multifunctional agent against uveal melanoma, J. Med. Chem. 64 (2021) 13622–13632, https://doi.org/10.1021/acs.jmedchem.1c00995.
[56] I. Cacciatore, L. Marinelli, E. Fornasari, L.S. Cerasa, P. Eusepi, H. Türkez, A. Di Stefano, Novel NSAID-derived drugs for the potential treatment of Alzheimer's disease, Int. J. Mol. Sci. 17 (2016) 1035, https://doi.org/10.3390/ijms17071035.
[57] X. Chen, A. Murawski, K. Patel, C.L. Crespi, P.V. Balimane, A novel design of artificial membrane for improving the PAMPA model, Pharm. Res. (N. Y.) 25 (2008) 1511–1520, https://doi.org/10.1007/s11095-007-9517-8.
[58] P. Sozio, L. Marinelli, I. Cacciatore, A. Fontana, H. Türkez, G. Giorgioni, A. Di Stefano, New flurbiprofen derivatives: synthesis, membrane affinity and evaluation of in vitro effect on β-amyloid levels, Molecules 18 (2013) 10747–10767, https://doi.org/10.3390/molecules180910747.
[59] I. Hubatsch, E. Ragnarsson, P. Artursson, Determination of drug permeability and prediction of drug absorption in Caco-2 monolayers, Nat. Protoc. 2 (2007) 2111–2119, https://doi.org/10.1038/nprot.2007.303.
[60] M. Markowska, R. Oberle, S. Juzwin, C.P. Hsu, M. Gryszkiewicz, A.J. Streeter, Optimizing Caco-2 cell monolayers to increase throughput in drug intestinal absorption analysis, J. Pharmacol. Toxicol. Methods 46 (2001) 51–55, https://doi.org/10.1016/S1056-8719(01)00161-7.